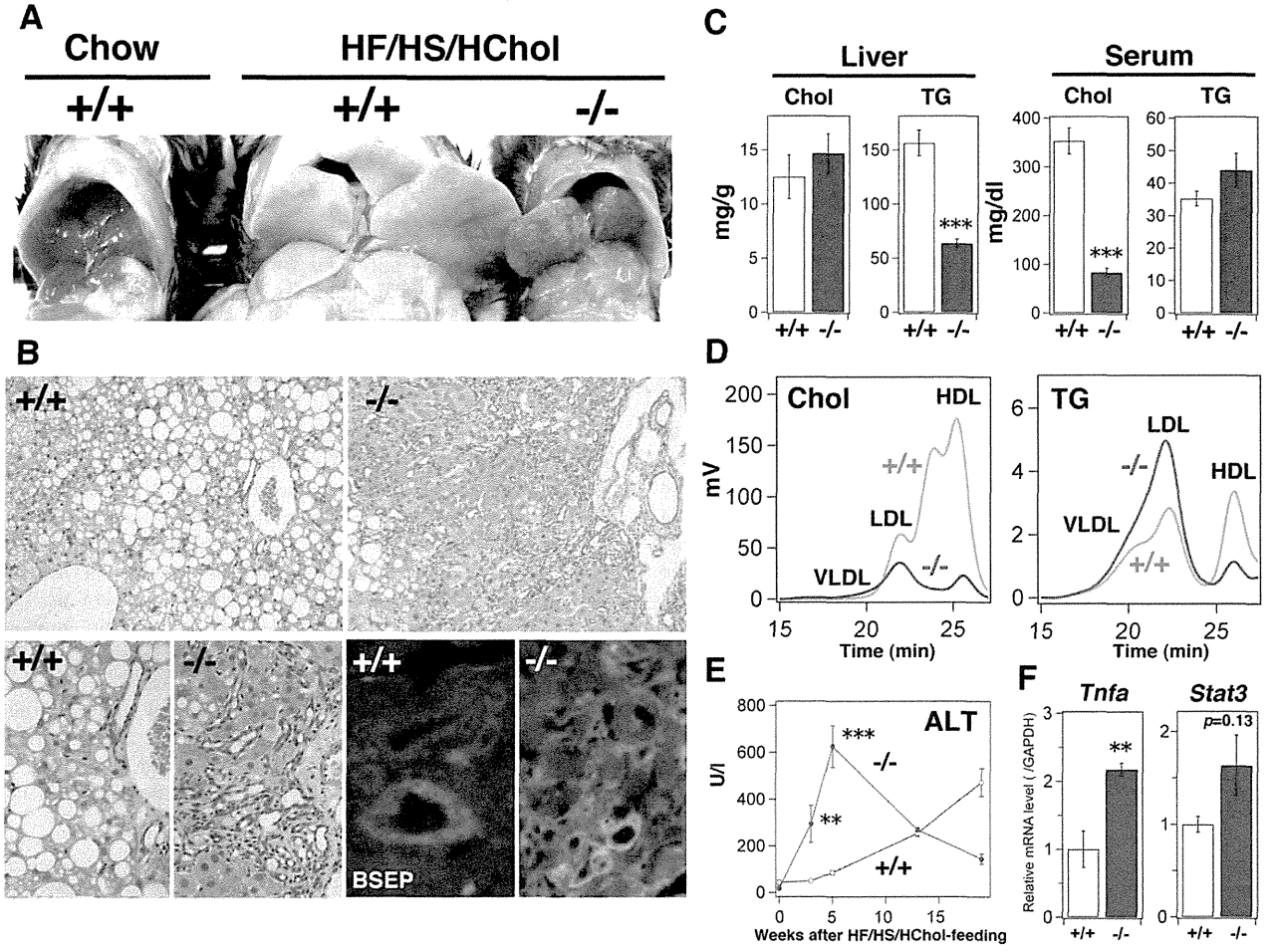

Figure 4. *Sik3*$^{-/-}$ mice are less tolerant to a cholesterol-containing high-fat diet. (A) Male mice were fed a high-fat and high-sucrose diet supplemented with 2% cholesterol (HF/HS/HChol) for 4 months (12–30 weeks) and then sacrificed (n = 6). (B) HE staining of the liver (sets at the *upper* and *lower left*), BSEP-staining (*lower right*: BSEP is green and nuclei are blue (DAPI)). The magnification is the same in each set. (C) Cholesterol and TG levels in the liver and serum were measured (n = 6). *** indicates $p<0.001$. Means and SEM are shown. (D) FPLC analysis of serum lipids. (E) Serum levels of alanine aminotransferase (ALT) were monitored at the indicated time points. ** indicates $p<0.01$. (F) Quantitative polymerase chain reaction analysis of inflammatory molecules (tumor necrosis factor-α and STAT3) in the liver.
doi:10.1371/journal.pone.0037803.g004

because cholesterol was depleted from the bile of *Sik3*$^{-/-}$ mice (Figure 7F); this could have been caused by the decreased levels of phospholipids followed by the reduced solubility of bile [41].

High serum BA and ALT levels were observed in *Sik3*$^{-/-}$ mice on the high-CA diet (Figure 7G). The levels of ALP and total bilirubin were also high in *Sik3*$^{-/-}$ mice (Figure 7H). The lipid droplets observed in the livers of *Sik3*$^{-/-}$ mice (Figure 7B) might be composed of cholesterol because cholesterol, and not TG, had accumulated in their livers (Figure 7I). The levels and patterns of serum cholesterol and TG in *Sik3*$^{-/-}$ mice were also abnormal (Figure 7J); notably, the levels of cholesterol in the VLDL-LDL fraction of the wild-type mice was enhanced by CA feeding, which was more obvious in *Sik3*$^{-/-}$ mice. Given the severe phenotype caused by CA feeding, we surmised that cholestasis might be the primary phenotype of *Sik3*$^{-/-}$ mice, and this may then lead to or enhance the other phenotypes, *e.g.*, lipodystrophy and dyslipidemia.

Because most of the *Sik3*$^{-/-}$ mice were dead on the day of birth (Figure S1A), we examined the livers of embryos. As shown in Figure S3A, hepatocytes in *Sik3*$^{-/-}$ embryos (E18.5) were not normal; notably, the hepatocytes were of a variable size, and a significant number of multinucleated hepatocytes were observed, suggesting liver damages due to embryonic cholestasis. It was partly true that the BA levels in the livers of *Sik3*$^{-/-}$ embryos were higher than those of wild-type embryos (Figure S3B). However, when the mice were born, the BA content in the liver of the wild-type mice reached levels equivalent to that of *Sik3*$^{-/-}$ mice and decreased thereafter, suggesting that hepatic cholestasis might occur in *Sik3*$^{-/-}$ embryos, but it cannot explain the early death of *Sik3*$^{-/-}$ mice. Alternatively, we suppose that *Sik3*$^{-/-}$ neonates may unable to adapt their metabolism to the environmental changes at birth.

Gene Expression Profile in the Livers of Sik3$^{-/-}$ Mice Fed with Special Diets

We examined mRNA expression in the liver to elucidate the mechanisms involved in the *Sik3*$^{-/-}$ phenotypes. As shown in Table S1, the resistance to diet-induced obesity in *Sik3*$^{-/-}$ mice might be explained by the low levels of lipogenic mRNA, *e.g.*, *Fasn* and *Scd1*. Amelioration of hepatic injury in *Sik3*$^{-/-}$ mice

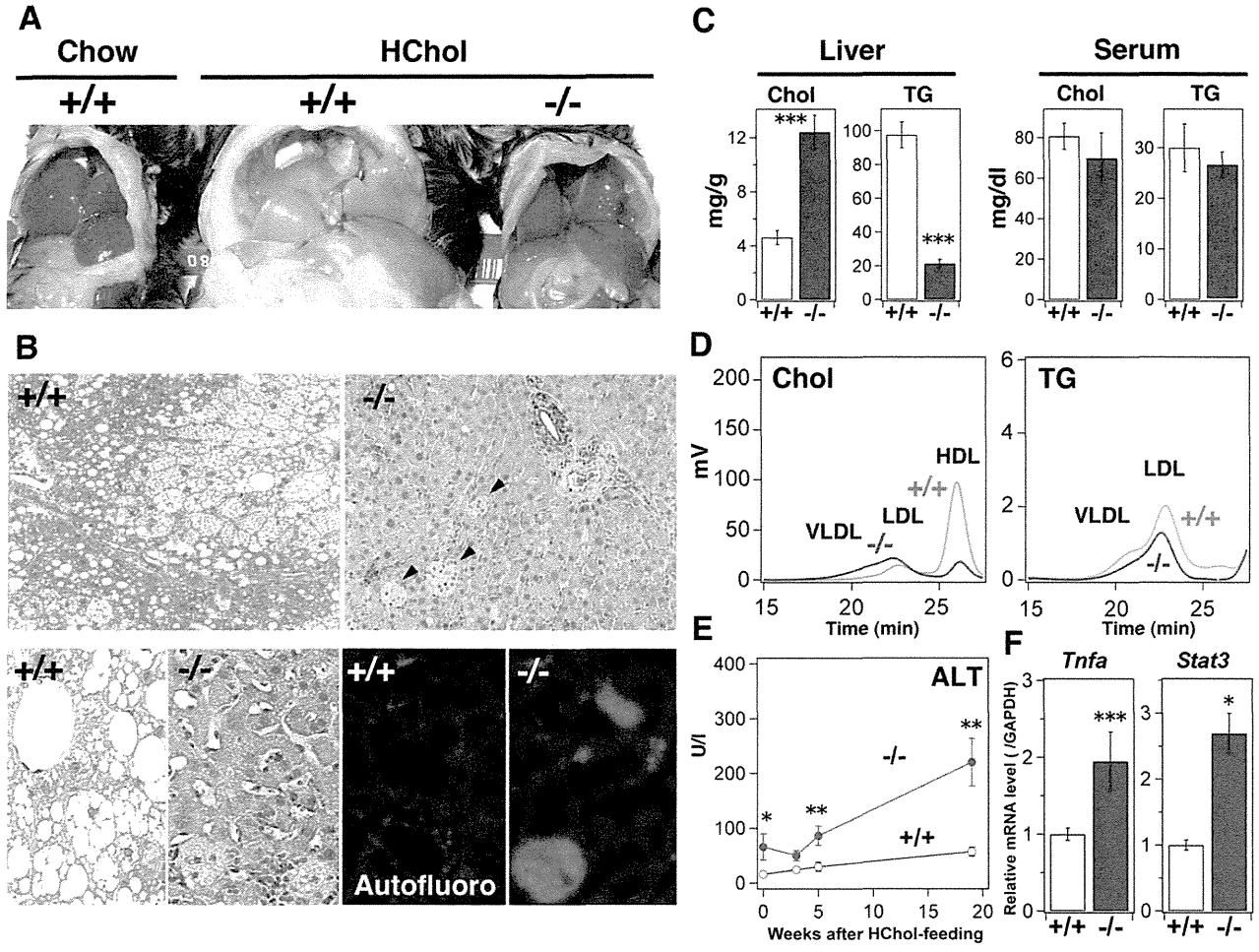

Figure 5. Cholesterol accumulation in the livers of *Sik3*$^{-/-}$ mice after feeding with a high-cholesterol diet. (A) Male mice were fed a 2% cholesterol diet for 4 months (12–30 weeks) and then sacrificed (n = 5). (B) HE staining of the liver (sets at the *upper* and *lower left*). The arrows indicate eosin-negative foci which with autofluorescence (*lower right*: red, and nuclei are blue (DAPI)). The magnification is the same in each set. (C) Cholesterol and TG levels in the liver and serum were measured (n = 5). *** indicates $p<0.001$. Means and SEM are shown. (D) FPLC analysis of serum lipids. (E) Serum levels of alanine aminotransferase (ALT) were monitored at the indicated time points. * and ** indicate $p<0.05$ and $p<0.01$, respectively. (F) Quantitative polymerase chain reaction analysis of inflammatory molecules in the liver.
doi:10.1371/journal.pone.0037803.g005

by the high-fat diet was probably due to the down-regulation of cholesterol (*HmgCoAr*) and BA (*Cyp7a*) synthesis.

However, the mRNA expression patterns of mice fed on the high-cholesterol or high-CA diet could not explain the pathogenesis of *Sik3*$^{-/-}$ *mice*, and some discrepancies remained. When mice were fed with the high-cholesterol diet, no significant difference in the mRNA levels of genes for cholesterol synthesis, *e.g.*, *HmgCoAr*, was observed between wild-type and *Sik3*$^{-/-}$ mice. The level of *Cyp7a* (bile acid synthesis) mRNA was also the same, despite the high expression level of its repressor (*Shp*). Meanwhile, when the mice were fed with the high-CA diet, *Sik3*$^{-/-}$ mice expressed lower levels of *Cyp7a* mRNA than the wild-type mice, despite no changes in the levels of *Shp*.

Here, we have to mention some of the problems associated with these gene expression analyses. For example, the mice that were fed the different diets were of different ages. In addition, the special diets were suspected to produce secondary effects, such as hepatic injury. Therefore, we decided to examine gene expression during the acute phase.

Adaptive Gene Expression is Dysregulated in Sik3$^{-/-}$ Mice

To examine gene expression during the acute phase with a biased diet, 12-week-old mice were fed either a high-cholesterol or high-CA diet for 2 days or a high-fat diet for 2 weeks. As shown in Figure 8A and S3A, the gene expression profile in the livers of young mice under chow-diet feeding was different from that of aged mice (Figure 3A), probably due to differences in the degree of hepatic injury (Figure 6A). Under the acute phase condition, the genes were categorized into 2 groups: (1) mRNA levels not affected by the diets in *Sik3*$^{-/-}$ mice (*e.g., Shp, Bsep, AbcG5, AbcA1, and Fasn)*, and (2) mRNA levels that were irregularly affected (*e.g., Cyp7a, Cyp8b,* and *Cyp27a)* (Figure 8A and S4A). Strangely, *Cyp7a* gene expression was lower in *Sik3*$^{-/-}$ mice than in wild-type mice, despite the low expression levels of *Shp*.

The little or no expression of *Cyp7a* observed under the high-cholesterol diet in *Sik3*$^{-/-}$ mice could be explained by LXR dysfunction [3], while the low expression of *Shp* or *Bsep* [6] and hypertrophic gallbladder [40] suggested FXR dysfunction. RXR is activated by 9-cis-RA, which is synthesized from vitamin A [9],

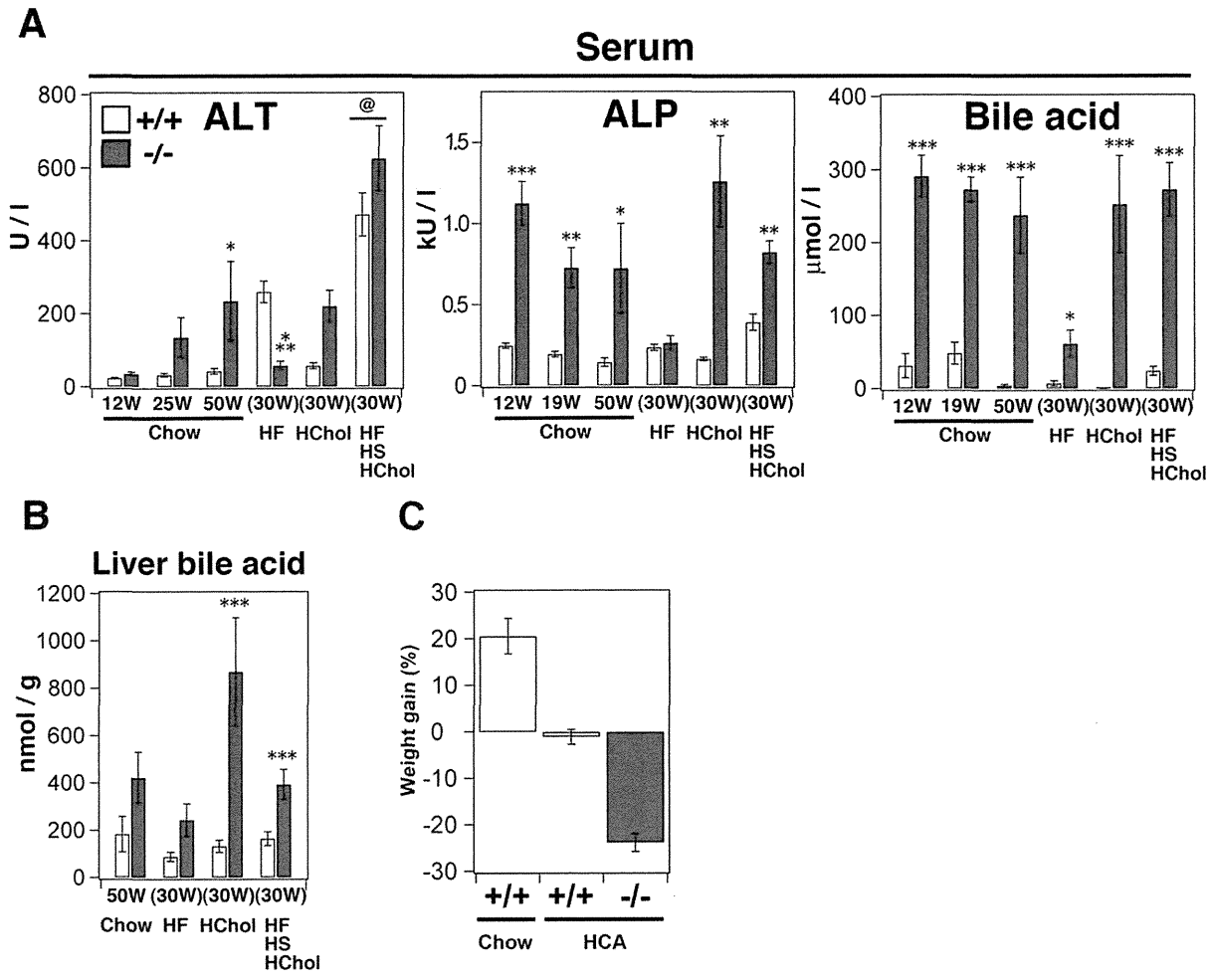

Figure 6. Excess bile acids in the serum and liver of *Sik3*$^{-/-}$ mice. (A) The serum levels of ALT, alkaline phosphatase, and bile acids are shown. The age at serum collection of the mice fed a chow diet (n = 4–6) are shown, while those of mice fed an HF, HChol, or HF/HS/HChol diet (n = 5–6) was 30 weeks (feeding 12–30 weeks). @ in the ALT panel indicates the maximum values for the results shown in Figure 4E. (B) Bile acids were extracted from the liver (n = 3) and normalized by liver weigh. (C) Gain of body weight after feeding mice with a high cholic acid (CA)-containing diet. Wild type (n = 6) and *Sik3*$^{-/-}$ mice (n = 5) were fed a diet supplemented with 0.25% CA for 1 month. For the control group, wild-type mice (n = 9) were fed with a chow diet.

doi:10.1371/journal.pone.0037803.g006

and the impairment of RXR function affects vitamin A metabolism [42], resulting in the proliferation of bile duct epithelial cells (Figure 4B) [43]. Moreover, the livers of *Sik3*$^{-/-}$ mice expressed lower levels of *Rxrα*mRNA than the livers of wild-type mice, when the mice were fed with diets rich in cholesterol or CA (Figure S4B). Therefore, we decided to examine vitamin A metabolism in the livers of *Sik3*$^{-/-}$ mice by quantifying mRNA and protein levels.

The mRNA and protein levels of *cellular retinoid-binding protein 1* (*Crbp1*) and *retinal aldehyde dehydrogenase 1a* (*Aldh1a*) were up- and down-regulated, respectively, in *Sik3*$^{-/-}$ mice (Figure S4C and 8B). *Aldh1a* mRNA levels in the livers of *Sik3*$^{-/-}$ mice were also unaffected by the diet (Figure 8C). In addition, the livers of *Sik3*$^{-/-}$ mice contained higher levels of free retinol (vitamin A) than the livers of wild-type mice (Figure 8D). Moreover, treatment with 9-cis-RA rapidly reduced the levels of free retinol in the livers of *Sik3*$^{-/-}$ mice compared to the wild-type mice, suggesting that vitamin A metabolism might be impaired in *Sik3*$^{-/-}$ mice.

To further characterize these findings, the mice were treated with 9-cis-RA for 7 days, and several phenotypic parameters were then examined. Because 9-cis-RA is a pleiotropic compound, we first determined the minimum dose of 9-cis-RA as 4 mg kg^{-1}·day^{-1} by monitoring the body weight and blood glucose levels of wild-type mice (Figure S5A and B). Treatment with 9-cis-RA induced weight gain in *Sik3*$^{-/-}$ mice (Figure 8E) and enabled them to maintain their blood glucose levels after fasting (Figure 8F). In addition, 9-cis-RA substantially decreased the levels of serum ALP and bile acid in *Sik3*$^{-/-}$ mice (Figure S5C). *Sik3*$^{-/-}$ mice treated with 9-cis-RA were also able to respond to nutritional stress by inducing the expression of metabolic markers (compare Figure 8G to 8A and Figure S5D). These results suggest that impaired vitamin A metabolism might be a cause of the phenotypes of *Sik3*$^{-/-}$ mice.

Discussion

Here, we have shown that SIK3 is induced in the liver when mice are fed a diet rich in fat, sucrose, and cholesterol. *Sik3*$^{-/-}$ mice present with a malnourished phenotype due to their reduced adaptation to excess nutrition, especially to cholesterol and CA,

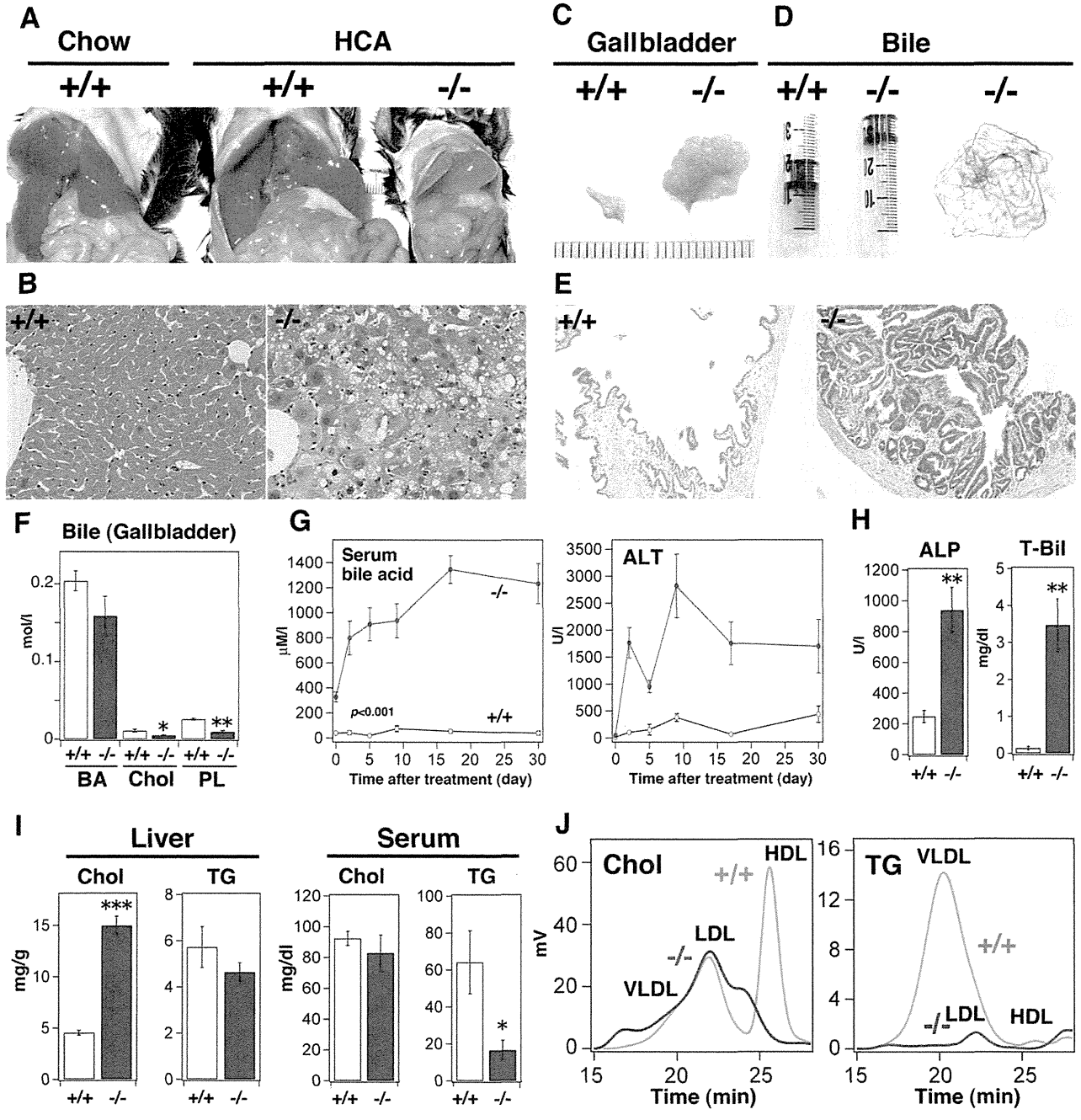

Figure 7. *Sik3*$^{-/-}$ mice are less tolerant to a cholic acid (CA)-containing diet. (A) Mice (n = 6, but *Sik3*$^{-/-}$ mouse died before 1 month) were fed a diet supplemented with 0.25% cholic acid for 1 month (12–16 weeks) and then sacrificed. (B) HE staining of the liver (*left*), BSEP staining (*right*: BSEP is green and nuclei are blue (DAPI)). The magnification is the same in each set. (C) Photographs of gallbladders (scale, 1 mm). (D) The color of bile juice and bile sand in the gallbladder. (E) HE staining of the gallbladder. The magnification is the same in both panels. (F) The levels of bile acid (BA), cholesterol (Chol), and phospholipids (PL) in bile juice from the gallbladder were measured. * and ** indicate $p<0.05$ and <0.01, respectively. Means and SEM are shown. (G) Serum BA and alanine aminotransferase (ALT) levels were monitored at the indicated periods. All ALT data points are $p<0.001$, except day 0. (H) Serum alkaline phosphatase (ALP) and total bilirubin (T-Bil) levels were measured. (I) Cholesterol and TG levels in the liver and serum were measured. *** indicates $p<0.001$. (J) FPLC analysis of serum lipids.
doi:10.1371/journal.pone.0037803.g007

which eventually leads to severe cholestasis. These phenotypes are continuously observed even after 10 generations of cross-breeding with normal C57BL/6J mice, and we observed no substantial difference between males and females in their response to biased diets. Given these results, we propose that SIK3, in combination with vitamin A metabolism, is a novel regulator of cholesterol-BA homeostasis and lipid-storage size (Figure 9).

Previous studies suggested a direct contribution of RXR to cholesterol-BA homeostasis. Because the RXR ligand 9-cis-RA is synthesized from vitamin A, which is absorbed from enterocytes

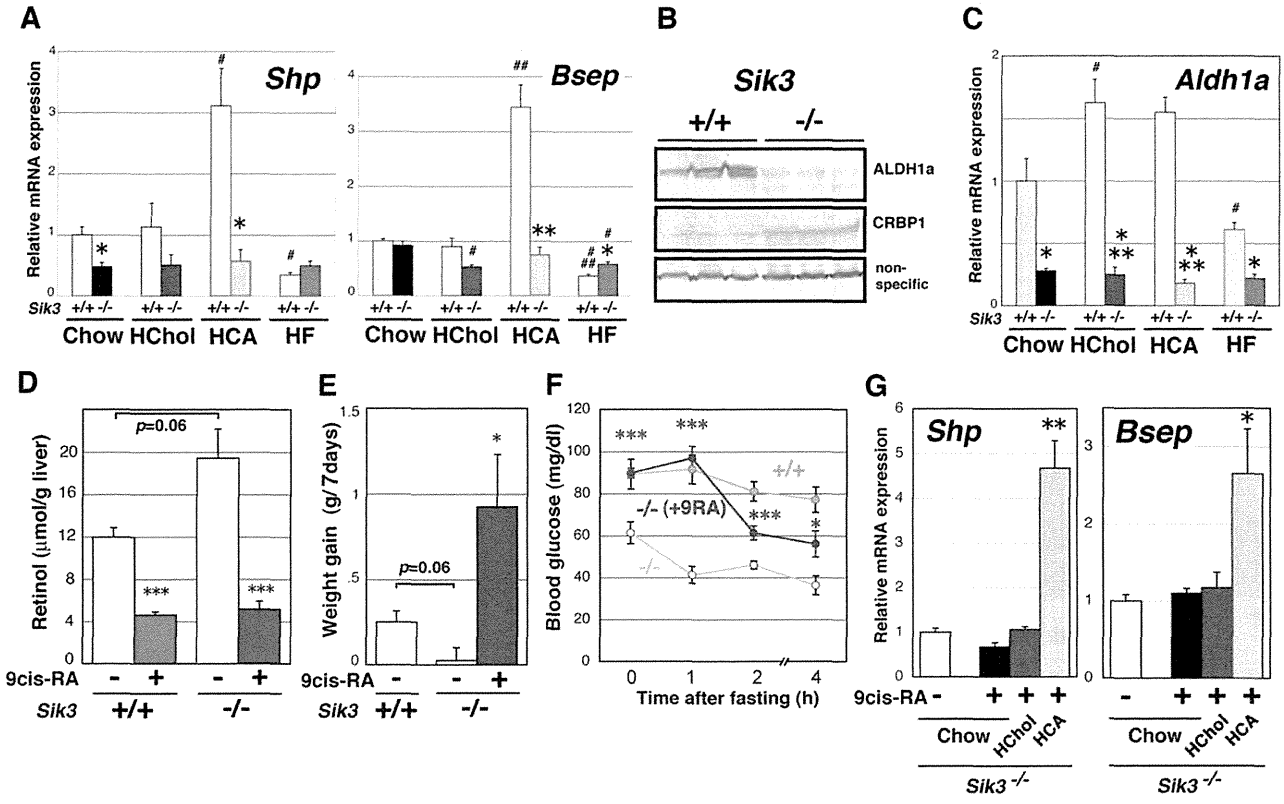

Figure 8. Impairment of cholesterol and bile acid (BA) metabolic gene regulation in *Sik3*$^{-/-}$ mice. (A) Male mice (12 weeks of age, n = 3) were fed diets supplemented with cholesterol (2%) and cholic acid (CA) (0.25%) for 2 days or with fat (60% of calories) for 2 weeks and then sacrificed. The expression of genes for cholesterol and BA metabolism in the liver was examined using qPCR (normalized by glyceraldehyde 3-phosphate dehydrogenase [*Gapdh*] levels). Significant differences between wild-type and *Sik3*$^{-/-}$ mice are shown by *, **, and *** for $p<0.05$, <0.01, and <0.001, respectively. # indicates significant differences between the chow and special diet groups. Means and SEM are shown. (B) Western blot analysis of ALDH1a and CRBP1 levels. (C) The levels of *Aldh1a* mRNA in mouse liver (normalized by *Gapdh* levels). (D) Levels of free retinol (vitamin A) in the livers of wild-type and *Sik3*$^{-/-}$ mice. Mice (12 weeks of age, n = 3) were treated with (+) or without (−) 9-cis-RA (8.3 mg/kg, suspended in 1% ethanol) intraperitoneally. After 6 h, the liver was recovered. (E) Mice (wild type, n = 4; *Sik3*$^{-/-}$ mice, without and with treatment, n = 4 and n = 12, respectively) were treated with 9-cis-RA (4 mg kg^{-1}·d^{-1}) for 7 days and the weight gain during this period is shown. * indicates a significant difference in the *Sik3*$^{-/-}$ groups. (F) After 7 days of treatment, the mice in each group were fasted and their blood glucose levels were monitored. Significance was calculated in the *Sik3*$^{-/-}$ groups. (G) At day 7, the *Sik3*$^{-/-}$ mice that were treated with RA were grouped into sets of 3 (n = 4) and fed a chow, high-cholesterol, or high-CA diet for a further 2 days under continuous RA treatment; mRNA levels in the liver were then examined. Significant differences between the chow and special diet groups are indicated.
doi:10.1371/journal.pone.0037803.g008

with the assistance of BA, its metabolism is tightly coupled to BA homeostasis [44]. A lack of vitamin A stimulates BA synthesis and its transport from hepatocytes to the bile ducts, *e.g.*, via *Cyp7a* and *Bsep* gene expression [45], while excess 9-cis-RA inhibits their expression. The reduced expression of ALDH1a, an RA synthase, in the livers of *Sik3*$^{-/-}$ mice might be one of the causes of the *Sik3*$^{-/-}$ phenotype. All-trans-RA suppresses the expression of *Aldh1a* via an RAR-dependent mechanism [46], but 9-cis-RA does not, suggesting a distinct action for 9-cis-RA from all-trans-RA. Because physiological/endogenous 9-cis-RA has been identified only in the pancreas [47,48], analyses of not only 9-cis-RA, but also its related substances in the liver are required to precisely characterize the *Sik3*$^{-/-}$ phenotype.

The administration of 9-cis-RA to *Sik3*$^{-/-}$ mice recovered the expression of *Cyp7a* and *Bsep* (Figure 7A and 7G), suggesting that the dose used (4 mg kg^{-1}·d^{-1}) may not be excessive for *Sik3*$^{-/-}$ mice. However, we have to mention that the wild-type mice that were fed with a vitamin A-deficient diet for 6 months from weaning did not develop cholestasis (unpublished observation), indicating that the levels of vitamin A and its metabolites may be insufficient to explain all of the *Sik3*$^{-/-}$ phenotypes. Meanwhile, free retinol (vitamin A) accumulated in the livers of *Sik3*$^{-/-}$ mice. Vitamin A toxicity is also suspected in hepatic cholestasis [49], suggesting that increased levels of free retinol may also contribute to the dysregulation of cholesterol-BA homeostasis in *Sik3*$^{-/-}$ mice. In addition, retinol aldehyde, a substrate of ALDH1a and a precursor of RA, is found to possess strong anti-obesity actions in mice [10].

Meanwhile, the high-fat diet ameliorated cholestasis in *Sik3*$^{-/-}$ mice (Figure 6A) without FA storage (in the liver and adipose tissues) or restoring the mRNA levels of genes involved in FA synthesis, such as *Fasn* (Figure 2 and Table S1). Interestingly, the high-fat diet up-regulated the expression of *thiolase*, a PPARα target, in the livers of *Sik3*$^{-/-}$ mice. PPARα is known to enhance bile flow [50] and some transcriptional pathways, such as *Shp* [51] (and also compare Table S1 to Figure 3A). Given that RXR is required for PPARα activation, its signaling may also be impaired in *Sik3*$^{-/-}$ mice, as expected from the gene expression profile observed for the chow diet (Figure 3A). These observations suggest that excess fat may stimulate a part of the downstream PPARα

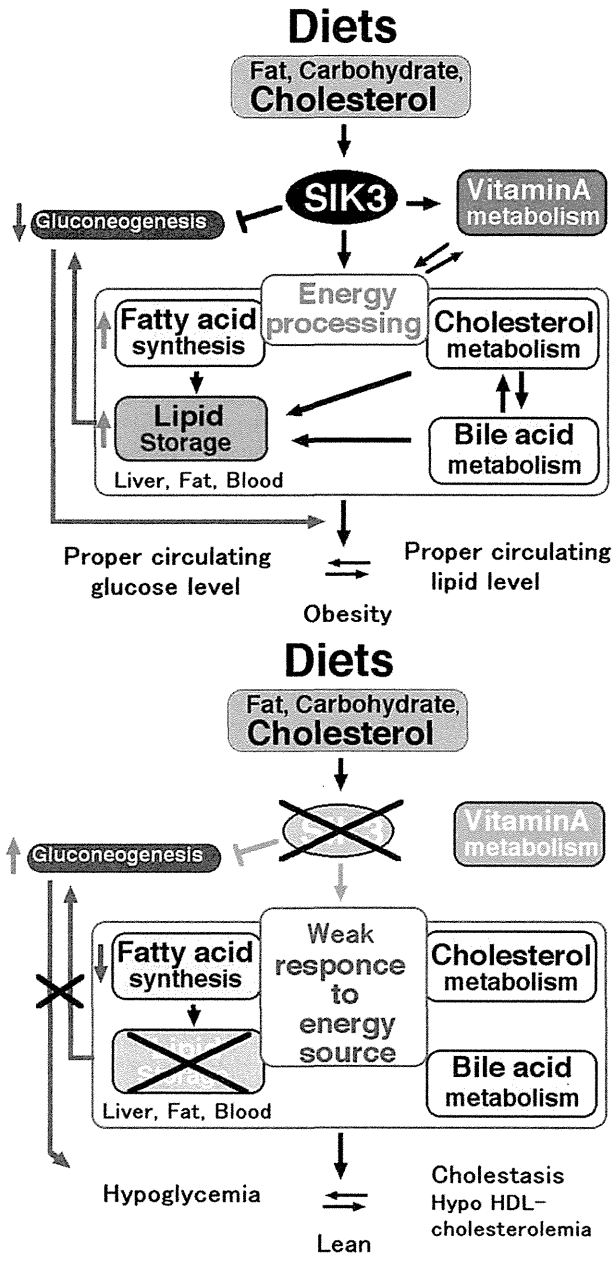

Figure 9. Summary of the metabolic events in wild-type (*upper*) and in *Sik3*$^{-/-}$ mice (*lower*).
doi:10.1371/journal.pone.0037803.g009

pathway (or close the gap downstream from PPARα that is impaired in *Sik3*$^{-/-}$ mice), which can improve BA homeostasis, probably in an SIK3-independent manner.

AMPK-related kinases are activated by the upstream kinase LKB1 [29,52] SIK3 or AMPK–which kinase is important for the LKB1-mediated suppression of gluconeogenesis in the liver? Loss of LKB1 in the liver enhances the gluconeogenic program [53]. Since the gluconeogenic program in LKB-defective mice is resistant to the AMPK activator metformin, AMPK is proposed to be the kinase responsible for the LKB1-mediated regulation of gluconeogenesis. However, the livers of *Sik3*$^{-/-}$ mice possessed activated AMPK and an enhanced gluconeogenic program (Figure 3B), suggesting that loss of LKB1 causes a deficiency of SIK3 and subsequent AMPK resistance. In addition to gluconeogenesis, liver-specific LKB-defective mice present with severe cholestasis due to a lack of BSEP membrane-localization in the liver [54], while the apical side of the dilated canalicular structure was positive for BSEP in the livers of *Sik3*$^{-/-}$ mice, suggesting that the cause of cholestasis in these mice may not be identical to that in LKB-defective mice. We would again emphasize that the high-fat diet ameliorated cholestasis in *Sik3*$^{-/-}$ mice, indicating the importance of the process for nutrients rather than developmental defects in BA transportation.

Two recent reports have provided an argument against mechanisms by which SIK3 regulates energy balance. Mihalova *et al.* found that class 2a HDACs activated the FOXO transcription factor via deacetylation, thereby up-regulating gluconeogenesis in the liver [37]. Conversely, Wang *et al.* reported that loss of SIK2 in *Drosophila* (by disrupting the fly's *Sik3* gene) resulted in the dephosphorylation of HDAC4 and the subsequent activation of FOXO [28]. Activated FOXO induces the lipolytic programs that reduce the lipid levels in body fat, thereby rendering the fly vulnerable to starvation. These data suggest that disinactivation of class 2a HDACs followed by the constitutive activation of FOXO may be a cause of the phenotypes of *Sik3*$^{-/-}$ mice.

Conversely, *Crebbp*$^{+/-}$ mice, with a mutant allele of the histone acetylase CREB-binding protein, displayed a phenotypes similar to that of *Sik3*$^{-/-}$ mice, *e.g.*, lipodystrophy, increased glucose tolerance, resistance to diet-induced obesity, and hyperadiponectinemia [55], suggesting that SIK3 may regulate energy balance by regulating acetylation states. The levels of adipose tissue and circulating blood lipids may be important for buffering cholesterol and protecting the liver from cholesterol toxicity, which in turn, increases the risk of obesity and hyperlipidemia (Figure 9).

In the present study, profiling the metabolic changes in *Sik3*$^{-/-}$ mice represents a new start to the study SIK and may also provide novel insights into the metabolic diseases caused by Western diets. Another remarkable phenotype of *Sik3*$^{-/-}$ mice is found in the differentiation of chondrocytes [31], and a number of interactions between energy metabolism and skeletal development have been reported, *e.g.*, insulin [56], leptin [57], adiponectin [58], osteocalcin [59,60], and inflammatory cytokines [61]. Further analyses of the cell autonomous functions of SIK3 and of systemic or developmental abnormalities in the organs for energy metabolicsm in *Sik3*$^{-/-}$ mice are needed.

Materials and Methods

Sik3$^{-/-}$ Mice

Embryonic stem cells derived from a C57BL/6N strain (RENKA) were used with the *Sik3*$^{-/-}$ mice. After mating the mice with C57BL/6J mice (CLEA Japan, Tokyo, Japan) for 3 generations, mouse colonies were expanded for experiments under chow and high-fat-diet feeding. After 7 generations of cross breeding, mice colonies were used for cholesterol and cholic acid experiments. *Sik3*$^{+/-}$ mice are now supplied by JCRB Laboratory Animal Resource Bank at the National Institute of Biomedical Innovation (No. nbio157). The experimental mouse protocols were approved by the ethics committee at the National Institute of Biomedical Innovation (assigned No. DS-20-56). The animals were maintained under standard conditions of light (0800–2000) and temperature (23°C, 50% humidity).

For tissue isolation, all mice were fasted for 4 h and then sacrificed within ±1 h of lights out. The chow diet, MF, was purchased from Oriental Yeast (Tokyo, Japan). The high-sucrose (20% cal), high-fat (60% cal), and high-fat (45% cal)/high-sucrose

(20% cal) diets were obtained from Research DIET Inc. (NJ, USA). We supplemented 2% cholesterol in the high-fat and high-fat/high-sucrose diets. To prepare the high-cholesterol and high-cholic acid (CA) diets, the chow diet was supplemented with 2% cholesterol or 0.25% CA, respectively. O_2 consumption was monitored using the Oxymax system (Columbus Instruments, Columbus, OH, USA).

The pre-fasting periods for the glucose tolerance test (GTT), insulin tolerance test (ITT), and lactate tolerance test (LTT) were 4, 2, and 24 h, respectively. We administered 1.5 g/kg glucose, 36 μg/kg insulin, and 1.5 g/kg lactate intraperitoneally for these tests, respectively.

Fractionation of Hepatic Parenchymal Cells and Non-parenchymal Cells

Under anesthesia by isoflurane, female C57BL/6J mice (12-week-old) were perfused with Hank's balanced salt solution containing 0.5 mM EGTA via inferior vena cava followed by perfusion with Liver Digestion Medium (Invitorgen). After the digestion, hepatic cells were suspended in Dulbecco's Modified Eagle Medium (DMEM) supplemented with 10% fetal bovine serum and centrifuged at 40×g for 2 minutes. The pellet was used for the parenchymal-cell fraction, and the supernatant was recovered by further centrifuged at 800×g for 5 min and used for non-parenchymal-cell fraction.

Reagents

Blood glucose and β-hydroxybutyrate were measured using a G-meter (Arkray, Kyoto, Japan) and Precision Xceed (Abbott, Abbott Park, IL, USA), respectively. Total cholesterol and triglyceride (TG) in sera were measured using a DryChem7000 (Fujifilm, Tokyo, Japan). Lipids in the liver or feces were extracted in 10 volumes of methanol:chloroform (1:2), dried under N_2 gas, suspended in 300 μL t-butyl alcohol:methanol:-Triton-X 100 (2:1:1, v/v), and quantified using kits (WAKO, Osaka, Japan). Serum insulin, leptin and adiponectin levels were measured using enzyme-linked immunosorbent assay kits from Shibayagi (Gunma, Japan), and low levels of insulin were measured with a low range kit from Morinaga (Tokyo, Japan), while free FA and BA levels were measured using kits from WAKO. Serum lipid separation by fast protein liquid chromatography (FPLC) was contracted to LipiSEARCH (Skylight Biotech, Akita, Japan). The anti-AMPK, anti-phospho-AMPK, and anti-HDAC5 antibodies were purchased from Cell Signaling (Boston, MA, USA), anti-BSEP antibody were from ABGENT (San Diego, CA, USA), while the anti-ALDH1a and anti-CRBP1 antibodies were obtained from Epitomics (Burlingame, CA, USA). The anti-CRTC2 antibody was described previously [29].

Quantitative Real-time PCR

Total RNA was extracted using an EZ1 RNA Universal Tissue Kit (Qiagen, Venlo Park, Netherlands), and cDNA was synthesized using a Transcriptor cDNA First Strand Synthesis Kit (Roche, Branford, CT, USA). PCR amplification was performed using Platinum Quantitative PCR SuperMix (Invitrogen). Since the level of the internal standard RNA, 36B4, was induced by the CA-rich diet, the expression levels of mRNA in the liver of mice fed with diets supplemented with CA or Chol were normalized using glyceraldehyde 3-phosphate dehydrogenase levels. Gene names, abbreviations and primer sequence used in the quantities PCR analysis are listed in Table S2.

Statistical Analysis

Student's *t*-test was used to assess all experimental data in Microsoft Excel. The mean and standard error of the mean (SEM) are shown.

Supporting Information

Figure S1 (A) Most *Sik3*$^{-/-}$ mice died on the first day after birth. The mating system and time of genotyping are indicated. The percentage and number of mice in the first column indicate the sum of neonates at day 1 and embryos at E17.5–E18.5. Neonates prepared by *in vitro* fertilization were delivered by cesarean section and living mice were counted without genotyping. However, ~50% of the mice disappeared by the second day, probably because they were eaten by the foster mice. (B) The difference in the body size of *Sik3*$^{-/-}$ mice became obvious after 2 weeks. (C) HE staining of gonadal fat of 1-year-old mice. (D) Cholesterol (Chol), triglyceride (TG), and carbohydrate (Carbo) content in feces (from 3 cages). Cholesterol and triglycerides were extracted with methanol/chloroform as described in the Materials and Methods. To extract undigested carbohydrates, the feces were re-digested with amylase at 37°C for 12 h, and the debris was removed by centrifugation. Carbohydrates were stained with a solution of 1 volume of 5% phenol and 5 volumes of sulfuric acid and then detected at 490 nm. (E) After fasting for 4-h fasting, the serum levels of free thyroid hormones (FT3 and FT4) were measured with an automated system for clinical assays. Serum thyroid stimulating hormone (TSH) levels were measured with an ELISA kit from Shibayagi Co., Ltd. (F) Insulin tolerance test (ITT). Mice (male n = 5) were fasted for 2 h and then treated intraperitoneally with 36 μg/kg insulin. All data points are $p<0.001$.
(TIF)

Figure S2 (A) Body weight curves of wild-type and *Sik3* heterozygous mice are also shown (n = 12). (B) Levels of *Sik3* mRNA in the livers, brown adipose tissues (BAT), and muscles of wild-type, heterozygous, and *Sik3*$^{-/-}$ mice (n = 3). The error bars indicate SEM. Levels of SIK3 protein in the livers of wild-type, heterozygous, and *Sik3*$^{-/-}$ mice. (C) Hepatic parenchymal and non-parenchymal cells were separated by centrifugation, and *Sik3* mRNA levels were examined by quantitative PCR. *Cyp7α*, *F4/80*, and *Desmin* were used as markers for parenchymal cells, Kupffer's cells (non-parenchymal), and hepatic stellate cells (non-parenchymal), respectively. (n = 3: means and SEM are shown). (D) *In vitro* adipocyte differentiation assay. Preadipocytes were prepared from gonadal fat pads using collagenase and then plated. When the cells reached confluence, the culture medium was changed to Dulbecco's Modified Eagle's Medium (high glucose) supplemented with rosiglitazone (Rosi: indicated concentration), and insulin (1 μg/mL). After 8 days (with changes of medium every 2 days), the cells were fixed with 4% paraformaldehyde and stained with Oil Red O. The high magnification images show cells that were differentiated using 3 μM rosiglitazone. (F) Serum adiponectin levels of the mice examined in Figure 3E. Means and SEM are shown. ### indicates $p<0.001$.
(TIF)

Figure S3 (A) HE staining of embryo livers. The sets in the left and right panels are the same magnification. The lower panels are a higher magnification of the upper panels. (B) Bile acid was extracted with 95% ethanol/0.5% NH_3-water. The numbers of mice (wild-type and *Sik3*$^{-/-}$) used for the assay were: E16.5, 11 and 6; E18.5, 16 and 3; P0, 9 and 5; and 12 weeks, 8 and 5, respectively. Means and SEM are shown. Significant differences

between wild-type and *Sik3*$^{-/-}$ mice are shown by * for $p<0.05$. ## indicates significant differences between P0 and E18.5 or 12 weeks in wild-type mice ($p<0.01$).
(TIF)

Figure S4 (A) Male mice (12 weeks of age, n = 3) were fed diets supplemented with Chol (2%) and cholic acid (0.25%) for 2 days or with fat (60% of calories) for 2 weeks and then sacrificed. The expression of genes for Chol and BA metabolism in the liver was examined using quantitative polymerase chain reaction (normalized by glyceraldehyde 3-phosphate dehydrogenase [GAPDH] levels). Significant differences between wild-type and *Sik3*$^{-/-}$ mice are shown by *, **, and *** for $p<0.05$, <0.01, and <0.001, respectively. # indicates a significant difference between the chow and special diet groups. Means and SEM are shown. (B) Expression levels of nuclear receptors. (C) The expression of genes involved in vitamin A metabolism was examined using the liver cDNA in Figure 3A (1-year-old mice, n = 5).
(TIF)

Figure S5 (A) Effect of 9-cis-RA treatment (0–16 mg $kg^{-1} \cdot d^{-1}$) on the weight gain of wild-type mice (n = 6). (B) Blood glucose levels before and after treatment are indicated by labels as B and A, respectively. (C) The levels of serum ALP and bile acids were measured before (labeled as B) and after (labeled as A) 9-cis-RA treatment (for 9 days: after the analysis shown in Figure 8E). Ethanol (EtOH, 1%) was used as a solvent. Significant differences before and after treatment in the same group (n = 4) are indicated. Although there were no significant fluctuations in the levels of bile acids, their levels decreased in all *Sik3*$^{-/-}$ mice after treatment. (D) Effect of 9-cis-RA on gene expression in *Sik3*$^{-/-}$ mice. At day 7, *Sik3*$^{-/-}$ mice treated with 9-cis-RA were grouped into sets of 3 (n = 4) and fed a chow, high-Chol, or high-CA diet for an additional 2 days under continuous RA treatment; mRNA levels in the liver were then examined. Significant differences between the chow and special diet groups are indicated.
(TIF)

Table S1 mRNA levels in the liver.
(XLS)

Table S2 List of primers used for quantitative-PCR.
(XLS)

Acknowledgments

We are grateful to Mrs. Junko Morita (NIBIO), Dr. Kazuomi Nakamura (Tottori University), Mrs. Keiko Takeoka (Osaka University), and Mr. Naohiro Hori (Kinki University) for their technical support. We also thank Drs. Mitsuhiro Okamoto (Tezukayama University), Yasuki Nonaka (Osaka Aoyama University), Miho Ohta (Souai University), and Alan F. Hofmann (University of California) for their advice.

Author Contributions

Conceived and designed the experiments: H. Takemori JM NT SI KK AB AS AH MN. Performed the experiments: H. Takemori TU YI OH AK MS TS SS JD KT KM EM TK MK. Analyzed the data: KA TK MO JN H. Takikawa TF JM NT SI KK AB AS AH MN. Contributed reagents/materials/analysis tools: H. Takikawa KK YN HK TT TN. Wrote the paper: H. Takemori.

References

1. Wagner M, Zollner G, Trauner M (2011) Nuclear receptors in liver disease. Hepatology 53: 1023–1034.
2. Willy PJ, Umesono K, Ong ES, Evans RM, Heyman RA, et al. (1995) LXR, a nuclear receptor that defines a distinct retinoid response pathway. Genes Dev 9: 1033–1045.
3. Peet DJ, Turley SD, Ma W, Janowski BA, Lobaccaro JM, et al. (1998) Cholesterol and bile acid metabolism are impaired in mice lacking the nuclear oxysterol receptor LXR alpha. Cell 93: 693–704.
4. Kalaany NY, Gauthier KC, Zavacki AM, Mammen PP, Kitazume T, et al. (2005) LXRs regulate the balance between fat storage and oxidation. Cell Metab 1: 231–244.
5. Makishima M, Okamoto AY, Repa JJ, Tu H, Learned RM, et al. (1999) Identification of a nuclear receptor for bile acids. Science 284: 1362–1365.
6. Sinal CJ, Tohkin M, Miyata M, Ward JM, Lambert G, et al. (2000) Targeted disruption of the nuclear receptor FXR/BAR impairs bile acid and lipid homeostasis. Cell 102: 731–744.
7. Watanabe M, Houten SM, Mataki C, Christoffolete MA, Kim BW, et al. (2006) Bile acids induce energy expenditure by promoting intracellular thyroid hormone activation. Nature 439: 484–489.
8. Watanabe M, Horai Y, Houten SM, Morimoto K, Sugizaki T, et al. (2011) Lowering bile acid pool size with a synthetic farnesoid X receptor (FXR) agonist induces obesity and diabetes through reduced energy expenditure. J Biol Chem 286: 26913–26920.
9. Heyman RA, Mangelsdorf DJ, Dyck JA, Stein RB, Eichele G, et al. (1992) 9-cis retinoic acid is a high affinity ligand for the retinoid X receptor. Cell 68: 397–406.
10. Ziouzenkova O, Orasanu G, Sharlach M, Akiyama TE, Berger JP, et al. (2007) Retinaldehyde represses adipogenesis and diet-induced obesity. Nat Med 13: 695–702.
11. Iqbal J, Hussain MM (2009) Intestinal lipid absorption. Am J Physiol Endocrinol Metab 296: E1183–1194.
12. Takemori H, Okamoto M (2008) Regulation of CREB-mediated gene expression by salt inducible kinase. J Steroid Biochem Mol Biol 108: 287–291.
13. Doi J, Takemori H, Lin X-z, Horike N, Katoh Y, et al. (2002) Salt-inducible kinase represses PKA-mediated activation of human cholesterol side chain cleavage cytochrome promoter through the CREB basic leucine zipper domain. J Biol Chem 277: 15629–15637.
14. Takemori H, Katoh Y, Horike N, Doi J, Okamoto M (2002) ACTH-induced nucleocytoplasmic translocation of salt-inducible kinase. Implication in the protein kinase A-activated gene transcription in mouse adrenocortical tumor cells. J Biol Chem 277: 42334–42343.
15. Koo SH, Flechner L, Qi L, Zhang X, Screaton RA, et al. (2005) The CREB Coactivator TORC2 is a Key Regulator of Fasting Glucose Metabolism. Nature 437: 1109–1111.
16. Uebi T, Tamura M, Horike N, Hashimoto YK, Takemori H (2010) Phosphorylation of the CREB-specific coactivator TORC2 at Ser(307) regulates its intracellular localization in COS-7 cells and in the mouse liver. Am J Physiol Endocrinol Metab 299: E413–425.
17. Muraoka M, Fukushima A, Viengchareun S, Lombes M, Kishi F, et al. (2009) Involvement of SIK2/TORC2 signaling cascade in the regulation of insulin-induced PGC-1alpha and UCP-1 gene expression in brown adipocytes. Am J Physiol Endocrinol Metab 296: E1430–1439.
18. Sasaki T, Takemori H, Yagita Y, Terasaki Y, Uebi T, et al. (2011) SIK2 is a key regulator for neuronal survival after ischemia via TORC1-CREB. Neuron 69: 106–119.
19. Horike N, Kumagai A, Shimono Y, Onishi T, Itoh Y, et al. (2010) Downregulation of SIK2 expression promotes the melanogenic program in mice. Pigment Cell Melanoma Res 23: 809–819.
20. Kumagai A, Horike N, Satoh Y, Uebi T, Sasaki T, et al. (2011) A Potent Inhibitor of SIK2, 3, 3′, 7-Trihydroxy-4′-Methoxyflavon (4′-O-Methylfisetin), Promotes Melanogenesis in B16F10 Melanoma Cells. PLoS One 6: e26148.
21. Altarejos JY, Montminy M (2011) CREB and the CRTC co-activators: sensors for hormonal and metabolic signals. Nat Rev Mol Cell Biol 12: 141–151.
22. Conkright MD, Canettieri G, Screaton R, Guzman E, Miraglia L, et al. (2003) TORCs: transducers of regulated CREB activity. Mol Cell 12: 413–423.
23. Iourgenko V, Zhang W, Mickanin C, Daly I, Jiang C, et al. (2003) Identification of a family of cAMP response element-binding protein coactivators by genome-scale functional analysis in mammalian cells. Proc Natl Acad Sci U S A 100: 12147–12152.
24. Screaton RA, Conkright MD, Katoh Y, Best JL, Canettieri G, et al. (2004) The CREB coactivator TORC2 functions as a calcium- and cAMP-sensitive coincidence detector. Cell 119: 61–74.
25. Katoh Y, Takemori H, Min L, Muraoka M, Doi J, et al. (2004) Salt-inducible kinase-1 represses cAMP response element-binding protein activity both in the nucleus and in the cytoplasm. Eur J Biochem 271: 4307–4319.
26. Bricambert J, Miranda J, Benhamed F, Girard J, Postic C, et al. (2010) Salt-inducible kinase 2 links transcriptional coactivator p300 phosphorylation to the prevention of ChREBP-dependent hepatic steatosis in mice. J Clin Invest 120: 4316–4331.
27. Berdeaux R, Goebel N, Banaszynski L, Takemori H, Wandless T, et al. (2007) SIK1 is a class II HDAC kinase that promotes survival of skeletal myocytes. Nat Med 13: 597–603.
28. Wang B, Moya N, Niessen S, Hoover H, Mihaylova MM, et al. (2011) A hormone-dependent module regulating energy balance. Cell 145: 596–606.

29. Katoh Y, Takemori H, Lin XZ, Tamura M, Muraoka M, et al. (2006) Silencing the constitutive active transcription factor CREB by the LKB1-SIK signaling cascade. Febs J 273: 2730–2748.
30. Hashimoto YK, Satoh T, Okamoto M, Takemori H (2008) Importance of autophosphorylation at Ser186 in the A-loop of salt inducible kinase 1 for its sustained kinase activity. J Cell Biochem 104: 1724–1739.
31. Sasagawa S, Takemori H, Uebi T, Ikegami D, Hiramatsu K, et al. (2012) SIK3 is essential for chondrocyte hypertrophy during skeletal development in mice. Development 139: 1153–1163.
32. Lanjuin A, Sengupta P (2002) Regulation of chemosensory receptor expression and sensory signaling by the KIN-29 Ser/Thr kinase. Neuron 33: 369–381.
33. Wang B, Goode J, Best J, Meltzer J, Schilman PE, et al. (2008) The insulin-regulated CREB coactivator TORC promotes stress resistance in Drosophila. Cell Metab 7: 434–444.
34. Hurov JB, Huang M, White LS, Lennerz J, Choi CS, et al. (2007) Loss of the Par-1b/MARK2 polarity kinase leads to increased metabolic rate, decreased adiposity, and insulin hypersensitivity in vivo. Proc Natl Acad Sci U S A 104: 5680–5685.
35. Lennerz JK, Hurov JB, White LS, Lewandowski KT, Prior JL, et al. (2010) Loss of Par-1a/MARK3/C-TAK1 kinase leads to reduced adiposity, resistance to hepatic steatosis, and defective gluconeogenesis. Mol Cell Biol 30: 5043–5056.
36. Inagaki T, Dutchak P, Zhao G, Ding X, Gautron L, et al. (2007) Endocrine regulation of the fasting response by PPARalpha-mediated induction of fibroblast growth factor 21. Cell Metab 5: 415–425.
37. Mihaylova MM, Vasquez DS, Ravnskjaer K, Denechaud PD, Yu RT, et al. (2011) Class IIa Histone Deacetylases Are Hormone-Activated Regulators of FOXO and Mammalian Glucose Homeostasis. Cell 145: 607–621.
38. Takemori H, Katoh-Hashimoto Y, Nakae J, Olson EN, Okamoto M (2009) Inactivation of HDAC5 by SIK1 in AICAR-treated C2C12 myoblasts. Endocr J 56: 121–130.
39. Kim JY, van de Wall E, Laplante M, Azzara A, Trujillo ME, et al. (2007) Obesity-associated improvements in metabolic profile through expansion of adipose tissue. J Clin Invest 117: 2621–2637.
40. Moschetta A, Bookout AL, Mangelsdorf DJ (2004) Prevention of cholesterol gallstone disease by FXR agonists in a mouse model. Nat Med 10: 1352–1358.
41. Moschetta A, vanBerge-Henegouwen GP, Portincasa P, Renooij WL, Groen AK, et al. (2001) Hydrophilic bile salts enhance differential distribution of sphingomyelin and phosphatidylcholine between micellar and vesicular phases: potential implications for their effects in vivo. J Hepatol 34: 492–499.
42. Gyamfi MA, He L, French SW, Damjanov I, Wan YJ (2008) Hepatocyte retinoid X receptor alpha-dependent regulation of lipid homeostasis and inflammatory cytokine expression contributes to alcohol-induced liver injury. J Pharmacol Exp Ther 324: 443–453.
43. Weiss B, Barshack I, Onaca N, Goldberg I, Berkovich Z, et al. (2010) Vitamin A deficiency associated with enhanced proliferation of bile duct epithelial cells in the rat. Isr Med Assoc J 12: 82–86.
44. Schmidt DR, Holmstrom SR, Fon Tacer K, Bookout AL, Kliewer SA, et al. (2010) Regulation of bile acid synthesis by fat-soluble vitamins A and D. J Biol Chem 285: 14486–14494.
45. Hoeke MO, Plass JR, Heegsma J, Geuken M, van Rijsbergen D, et al. (2009) Low retinol levels differentially modulate bile salt-induced expression of human and mouse hepatic bile salt transporters. Hepatology 49: 151–159.
46. Elizondo G, Corchero J, Sterneck E, Gonzalez FJ (2000) Feedback inhibition of the retinaldehyde dehydrogenase gene ALDH1 by retinoic acid through retinoic acid receptor alpha and CCAAT/enhancer-binding protein beta. J Biol Chem 275: 39747–39753.
47. Kane MA, Folias AE, Pingitore A, Perri M, Obrochta KM, et al. (2010) Identification of 9-cis-retinoic acid as a pancreas-specific autacoid that attenuates glucose-stimulated insulin secretion. Proc Natl Acad Sci U S A 107: 21884–21889.
48. Kane MA (2012) Analysis, occurrence, and function of 9-cis-retinoic acid. Biochim Biophys Acta 1821: 10–20. pp 10–20.
49. Erickson JM, Mawson AR (2000) Possible role of endogenous retinoid (Vitamin A) toxicity in the pathophysiology of primary biliary cirrhosis. J Theor Biol 206: 47–54.
50. Kok T, Bloks VW, Wolters H, Havinga R, Jansen PL, et al. (2003) Peroxisome proliferator-activated receptor alpha (PPARalpha)-mediated regulation of multidrug resistance 2 (Mdr2) expression and function in mice. Biochem J 369: 539–547.
51. Chanda D, Lee CH, Kim YH, Noh JR, Kim DK, et al. (2009) Fenofibrate differentially regulates plasminogen activator inhibitor-1 gene expression via adenosine monophosphate-activated protein kinase-dependent induction of orphan nuclear receptor small heterodimer partner. Hepatology 50: 880–892.
52. Lizcano JM, Goransson O, Toth R, Deak M, Morrice NA, et al. (2004) LKB1 is a master kinase that activates 13 kinases of the AMPK subfamily, including MARK/PAR-1. Embo J 23: 833–843.
53. Shaw RJ, Lamia KA, Vasquez D, Koo SH, Bardeesy N, et al. (2005) The kinase LKB1 mediates glucose homeostasis in liver and therapeutic effects of metformin. Science 310: 1642–1646.
54. Woods A, Heslegrave AJ, Muckett PJ, Levene AP, Clements M, et al. (2011) LKB1 is required for hepatic bile acid transport and canalicular membrane integrity in mice. Biochem J 434: 49–60.
55. Yamauchi T, Kamon J, Minokoshi Y, Ito Y, Waki H, et al. (2002) Adiponectin stimulates glucose utilization and fatty-acid oxidation by activating AMP-activated protein kinase. Nat Med 8: 1288–1295.
56. Wu S, Aguilar AL, Ostrow V, De Luca F (2011) Insulin resistance secondary to a high-fat diet stimulates longitudinal bone growth and growth plate chondrogenesis in mice. Endocrinology 152: 468–475.
57. Yadav VK, Oury F, Suda N, Liu ZW, Gao XB, et al. (2009) A serotonin-dependent mechanism explains the leptin regulation of bone mass, appetite, and energy expenditure. Cell 138: 976–989.
58. Maeda T, Jikko A, Abe M, Yokohama-Tamaki T, Akiyama H, et al. (2006) Cartducin, a paralog of Acrp30/adiponectin, is induced during chondrogenic differentiation and promotes proliferation of chondrogenic precursors and chondrocytes. J Cell Physiol 206: 537–544.
59. Ferron M, Wei J, Yoshizawa T, Del Fattore A, DePinho RA, et al. (2010) Insulin signaling in osteoblasts integrates bone remodeling and energy metabolism. Cell 142: 296–308.
60. Fulzele K, Riddle RC, DiGirolamo DJ, Cao X, Wan C, et al. (2010) Insulin receptor signaling in osteoblasts regulates postnatal bone acquisition and body composition. Cell 142: 309–319.
61. Shikhman AR, Brinson DC, Valbracht J, Lotz MK (2001) Cytokine regulation of facilitated glucose transport in human articular chondrocytes. J Immunol 167: 7001–7008.

Molecular Genetics and Metabolism 106 (2012) 92–98

Contents lists available at SciVerse ScienceDirect

Molecular Genetics and Metabolism

journal homepage: www.elsevier.com/locate/ymgme

Therapeutic chaperone effect of *N*-Octyl 4-Epi-β-valienamine on murine G_{M1}-gangliosidosis

Yoshiyuki Suzuki [a,*], Satoshi Ichinomiya [a,c], Mieko Kurosawa [b], Junichiro Matsuda [d], Seiichiro Ogawa [e], Masami Iida [f], Takatoshi Kubo [f], Miho Tabe [g], Masayuki Itoh [h], Katsumi Higaki [i], Eiji Nanba [i], Kousaku Ohno [j]

[a] *Graduate School, International University of Health and Welfare, Otawara, Japan*
[b] *Center for Medical Science, International University of Health and Welfare, Otawara, Japan*
[c] *Department of Rehabilitation, Otawara Red Cross Hospital, Otawara, Japan*
[d] *Biological Resource Division, National Institute of Biomedical Innovation, Ibaraki City, Osaka, Japan*
[e] *Department of Biosciences and Informatics, Faculty of Science and Technology, Keio University, Yokohama, Japan*
[f] *Central Research Laboratories, Seikagaku Corporation, Higashi-Yamato, Japan*
[g] *Biochemistry Section, Analysis Center for Medical Science, SRL Inc, Hachioji, Japan*
[h] *Department of Mental Retardation and Birth Defect Research, National Institute of Neuroscience, National Center of Neurology and Psychiatry, Kodaira, Japan*
[i] *Division of Functional Genomics, Research Center for Bioscience and Technology, Tottori University, Yonago, Japan*
[j] *Division of Child Neurology, Faculty of Medicine, Tottori University, Yonago, Japan*

ARTICLE INFO

Article history:
Received 9 January 2012
Received in revised form 21 February 2012
Accepted 21 February 2012
Available online 3 March 2012

Keywords:
Chaperone therapy
G_{M1}-gangliosidosis
β-Galactosidase
N-octyl 4-epi-β-valienamine
NOEV

ABSTRACT

Therapeutic chaperone effect of a valienamine derivative *N*-octyl 4-epi-β-valienamine (NOEV) was studied in G_{M1}-gangliosidosis model mice. Phamacokinetic analysis revealed rapid intestinal absorption and renal excretion after oral administration. Intracellular accumulation was not observed after continuous treatment. NOEV was delivered to the central nervous system through the blood–brain barrier to induce high expression of the apparently deficient β-galactosidase activity. NOEV treatment starting at the early stage of disease resulted in remarkable arrest of neurological progression within a few months. Survival time was significantly prolonged. This result suggests that NOEV chaperone therapy will be clinically effective for prevention of neuronal damage if started early in life hopefully also in human patients with G_{M1}-gangliosidosis.

1. Introduction

G_{M1}-gangliosidosis (OMIM 230500) is one of the lysosomal diseases caused by mutations of the gene *GLB1* coding for β-galactosidase (β-gal) (EC 3.2.1.23) [1] with storage of ganglioside G_{M1}, keratan sulfate, and glycoprotein-derived oligosaccharides, presenting clinically with progressive neurological deterioration mainly in infancy (infantile form) and childhood (juvenile form), and rarely in adults (adult form) [2]. Morquio B disease (OMIM 253010) is another rare disease with skeletal manifestations without involvement of the central nervous system. These clinical forms are caused by different mutations of the same gene *GLB1* [3,4]. There is a correlation between the residual enzyme activity and severity of clinical phenotype, particularly the age of onset [5]. This finding led us to search for a molecular strategy to restore the apparently lost function of the mutant enzyme molecule. Soon a molecular instability was found in some mutant enzymes at relatively high environmental temperature and high pH [6,7].

Then a paradoxical phenomenon was found wherein a high amount of free galactose enhanced remarkably the intracellular mutant α-galactosidase A enzyme activity in cultured lymphoblasts from Fabry disease patients [8]. This observation was confirmed in a short-term human experiment [9]. A galactose analog 1-deoxygalactonojirimycin (DGJ) also was found to be effective in Fabry disease cells and tissues [10]. We concluded that low molecular weight competitive inhibitors could serve as chemical chaperones to induce expression of catalytic activities of mutant enzymes after stabilization and successful intracellular transport to the lysosome in somatic cells [11].

Subsequently we developed two derivatives of a newly synthesized organic compound valienamine, *N*-octyl 4-epi-β-valienamine (NOEV) and its epimer *N*-octyl β-valienamine as chemical chaperones for mutant β-galactosidase and β-glucosidase proteins, respectively, to restore the enzyme activities in somatic cells from patients with G_{M1}-gangliosidosis and Gaucher disease [12,13]. We focused our interest on NOEV for treatment and prevention of brain damage

Abbreviations: β-gal, β-galactosidase; NOEV, *N*-octyl 4-epi-β-valienamine; DGJ, 1-deoxygalactonojirimycin; WT, wild type; KO, knockout; Tg, transgenic; LC, liquid chromatography; MS/MS, tandem mass spectrometry; LLOQ, lower limit of quantification; GOT, glutamic-oxalacetic transaminase; GPT, glutamic-pyruvic transaminase; BUN, blood urea nitrogen; PBS, phosphate-buffered saline; BSA, bovine serum albumin.

* Corresponding author at: International University of Health and Welfare, Graduate School, 2600-1 Kita Kanemaru, Otawara 324-8501, Japan. Fax: +81 287 24 3229.
E-mail address: suzukiy@iuhw.ac.jp (Y. Suzuki).

1096-7192/$ – see front matter © 2012 Elsevier Inc. All rights reserved.
doi:10.1016/j.ymgme.2012.02.012

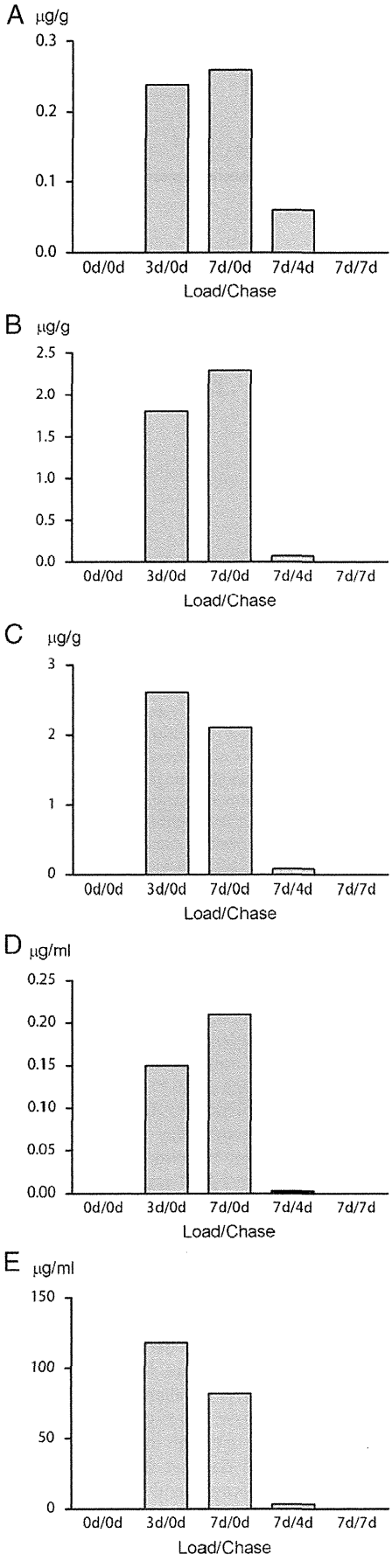

in G_{M1}-gangliosidosis, a classical neurogenetic disease in children [14]. In this article we report our experimental results of the therapeutic chaperone effect of NOEV on G_{M1}-gangliosidosis model mice. A preliminary result was published previously in a short report [15].

2. Materials and methods

2.1. NOEV synthesis and characterization

NOEV was synthesized essentially by the method described in a previous report [14]. In short, a glucocerebrosidase inhibitor [16,17] was modified by replacing the ceramide moiety with simple aliphatic chains [12,18] and multi-step epimerization at C-4 [13] to produce 4-epi-β-valienamine. In this study we used its *N*-octyl derivative, NOEV, for chaperone therapy experiments in murine G_{M1}-gangliosidosis. Its structure was assigned by a combination of COSY, TOCSY and HSQC NMR spectroscopy [14]. Then physicochemical properties were examined of molecular stability, solubility, and reactions with acids. In addition, analogous derivatives with various carbohydrate side chains were synthesized in order to evaluate relative chaperone activities.

2.2. G_{M1}-gangliosidosis model mice

We maintained a β-gal knockout (KO)-based transgenic (Tg) mouse strain overexpressing p.R201C mutant human β-gal, causing juvenile G_{M1}-gangliosidosis in humans (R201C Tg mouse; residual enzyme activity 4% of control) [14,19]. The genotype of newborn animals was confirmed by genomic analysis [14]. Wild-type (WT) mice (C57BL/6Cr) were purchased from Japan SLC (Shizuoka, Japan). The animals were kept in a temperature-controlled room (23 ± 1 °C) that was illuminated between 08:00 h. and 20:00 h. Commercial rodent chow and tap water were provided ad libitum. Body weight and fluid intake were regularly monitored.

All procedures were carried out in accordance with the Guide for Care and Use of Laboratory Animals by the National Institutes of Health, and were approved by the Animal Experiment Ethical Committees of National Institute of Biomedical Innovation, International University of Health and Welfare, Tottori University, National Institute of Neuroscience, and Seikagaku Corporation.

2.3. NOEV administration to model mice

An aqueous solution of NOEV (0.1–10 mM) was given ad libitum orally to the R201C Tg mouse. In some experiments the NOEV solution was given by gavage. The dose of daily NOEV administration was estimated by the body weight and amount of daily fluid intake. The mouse was clinically assessed regularly till the time of natural death or sacrifice followed by postmortem analysis.

2.4. NOEV determination

Tissue homogenates (20% w/v in water) were deproteinized with methanol. The supernatant was separated by centrifugation, and subjected to a combined liquid chromatography (LC) and tandem mass spectrometry (MS/MS) system (LC-MS/MS), consisting of an Agilent 1100 series quaternary pump and a thermostated column compartment at 40 °C (Agilent Technologies, Palo Alto, CA), HTS Autosampler, (Model 3133; Shiseido, Tokyo), and 4000 QTRAP mass spectrometer

Fig. 1. NOEV loading (1 mM oral, ad libitum) up to 7 days, followed by chase with water up to 7 days (WT mice, N = 2). NOEV concentrations were determined in the brain (A), liver (B), kidney (C), plasma (D), and urine (E). Each value is the mean concentration of two mouse tissues. LLOQ was 26.3 ng/ml (brain, liver, kidney), 5.25 ng/mg (plasma), or 506 ng/ml (urine). 0 d/0 d = no NOEV load, 3 d/0 d = NOEV load for 3 days without water chase, 7 d/0 d = NOEV load for 7 days without water chase, 7 d/4 d = NOEV load for 7 days followed by water chase for 4 days, 7 d/7 d = NOEV load for 7 days followed by water chase for 7 days.

(AB SCIEX, Foster City, CA). LC separation was carried out on a C18 (Atlantis dC18, particle size 5 μm; 50×2.1 mm) column (Waters, Milford, MA) with the mobile phase of methanol/10 mM ammonium formate (45/55 or 50/50, v/v). The flow rate was 0.2 ml/min, and the injection volume was 5 μl. The LC-MS/MS analyses were performed using a turbo ion spray interface and the positive ion multiple reaction monitoring mode. The lower limits of quantification (LLOQ) are indicated in Fig. 1 and Table 2.

2.5. β-Gal assay

The tissues were collected and directly frozen at −80 °C before use. β-Gal was assayed using 4-methylumbelliferyl β-galactopyranoside (Nacalai Tesque, Kyoto) [20]. Tissues were homogenized with 0.1% Triton X-100 in dH_2O. After centrifugation to remove insoluble materials, 10 μl of lysates with 20 μl of the substrate solution in 0.1 M citrate buffer (pH 4.5) was incubated at 37 °C for 30 min, and the reaction was terminated by adding 0.2 M glycine–NaOH buffer (pH 10.7). The liberated 4-methylumbelliferone was measured with a fluorescence plate reader (excitation 340 nm; emission 460 nm; Infinite F500, TECAN Japan, Kawasaki, Japan). Protein concentration was determined using a Protein Assay Rapid Kit (Wako, Tokyo, Japan).

2.6. Clinical assessment

We used three motor assessment tests in this study (Table 1): tail posture, tail suspension [21], and misstep on wire mesh to judge gripping power and strength [22]. They are easy to perform without special equipment for testing. Each test was scored into 4 grades (0–3) based on severity of abnormality. The highest total score was 9 for those with the most severe neurological abnormalities. Reliability and reproducibility of this test method were established [23]. GraphPad Prism 5 (GraphPad Software, La Jolla, CA, USA) was used for statistical analysis of two-way ANOVA (neurological course) and Gehan–Breslow–Wilcoxon Test (survival time).

2.7. Blood chemistry and urinalysis

Blood was collected by cardiac puncture in a heparinized tube, and plasma was separated by centrifugation. Urine was collected by external pressure or direct puncture of the bladder. The samples were kept frozen at −80 °C before use. Plasma was analyzed using FUJI DRI-CHEM 3000 V (Fuji Film, Tokyo) for glutamic-oxalacetic transaminase (GOT), glutamic-pyruvic transaminase (GPT), lactate dehydrogenase, blood urea nitrogen (BUN), creatinine, total protein, albumin, leucine aminopeptidase, alkaline phosphatase, total glyceride, total cholesterol, glucose, creatine kinase, and calcium. Urinalysis was performed using Uro-Labstix SG-L (Bayer Medical Ltd., Tokyo) for specific gravity, pH, protein, glucose, ketone bodies, urobilinogen, occult blood, and leukocytes.

2.8. General pathology and neuropathology

The animals were deeply anesthetized with diethyl ether before dissection and body fluid collection. For morphological studies, they were perfused through the heart with 4% phosphate-buffered paraformaldehyde. Then the tissues were collected for general pathology, neuropathology and immunohistochemistry [14,15].

Semi-quantitative histochemical assessment of ganglioside G_{M1} was performed as reported in a previous study [14]. Brain tissue sections were permeabilized with 0.25% Triton X-100 in phosphate-buffered saline (PBS) for 15 min at room temperature, blocked with 1% bovine serum albumin (BSA) in PBS for 1 h at room temperature, and incubated with monoclonal anti-G_{M1} antibody (clone GMB16) (Seikagaku, Tokyo, Japan) at 4 °C overnight. The sections were washed with 1% BSA in PBS 3 times for 5 min each at room temperature. They were then incubated with FITC-conjugated anti-mouse IgM, washed with PBS 3 times for 5 min each, and mounted on a slide glass [24]. Randomly selected 10 microscopic areas ($500\times500\ \mu m^2$) were subjected to fluorometric analysis, using Leica Confocal Software (Leica, Heidelberg) operated on the TCS SP2 confocal laser spectroscope (Leica, Wetzlar). Results of pathological examination were graded into 4 or 5 scores according to severity of findings in each tissue (Table 4).

3. Results

3.1. Physicochemical properties of NOEV

NOEV is an *N*-octyl derivative of galacto-type 4-epimer of valienamine, with N instead of O at C-1, and binding between C-1 and C-5 with C instead of O in the galactose core structure [5,13,25]. The chemical formula is $C_{15}H_{29}NO_4$ and molecular weight is 287.40.

It is an optically active unitary substance; colorless, oily, and hygroscopic; stable at dark place at room temperature and in vacuum; soluble in water, methanol, and ethanol; not soluble in chloroform. It reacts with CO_2 to form carbonate salt, and reacts with acids to form hydrochloride, sulfate, acetate, and citrate salts. The hydrochloride salt is white powder and hygroscopic. In this study we used the hydrochloride salt for all experiments. We tested compounds with carbohydrate chains of various lengths. *N*-octyl derivative showed the highest chaperone effect among them (data not shown).

3.2. Blood NOEV concentrations after single dose administration

Two different doses were given to WT mice for the time course study of blood concentrations after single gavage of 3 mg/kg (10 ml/kg) or 1.5 mg/kg (5 ml/kg) each of 1 mM free NOEV or hydrochloride salt solution (Table 2). Pharmacokinetic parameters were calculated, indicating that C_{max} and AUC were higher in the 3 mg/kg groups as compared to the 1.5 mg/kg groups. Higher water solubility of the hydrochloride salt resulted in more effective absorption as compared to free NOEV in the blood of mice in this study.

3.3. Tissue NOEV concentrations

Tissue distribution of NOEV was studied in WT mouse tissues and body fluids after short-term ad libitum oral administration of 1 mM NOEV (hydrochloride) solution (Fig. 1). NOEV was loaded for 3–7 days, followed by washout by administration of water without

Table 1
Motor assessment of G_{M1}-gangliosidosis model mice.

Test	Tail posture	Tail suspension	Misstep
Handling and observation	Rigidity and elevation	Response of hind limbs similar to parachute reflex in human infants	Stepping and walking on horizontal wire mesh for 30 s[a]
Score 0	Normal	Normal extension and abduction of hind limbs >45°,	No misstep for 30 s
Score 1	Slight elevation <20°	Hind limb abduction <45°	Misstep at 21–30 s
Score 2	Persistent elevation 20–45°	Minimal response of extension and abduction	Misstep at 11–20 s
Score 3	Persistent elevation >45°	Persistent flexion and adduction of hind limbs	Misstep at <10 s

[a] Mesh size 23.5×23.5 cm; mesh 2×2 cm.

Table 2
Pharmacokinetics of NOEV administration.

	C_{max} (ng/ml)	T_{max} (min)	$T_{½}$ (min)	$AUC_{0-\infty}$ (ng-min/ml)	AUC/D (ng-min-kg/ml/ng)	$MRT_{0-\infty}$ (min)
Free NOEV (3 mg/kg, $N=2$)	501.5	60.0	86.5	94,703	0.03	149.0
HCl salt (3 mg/kg, $N=4$)	664.0	60.0	112.3	144,037	0.05	186.5
Free NOEV (1.5 mg/kg, $N=2$)	259.2	30.0	76.0	45,996	0.03	127.1
HCl salt (1.5 mg/kg, $N=2$)	368.6	45.0	77.9	50,346	0.03	121.2

C_{max} = peak blood concentration; T_{max} = time to reach C_{max}; $T_{½}$ = elimination half-life; MRT = mean residence time; AUC = area under the blood concentration–time curve; AUC/D = AUC/dose. LLOQ = 24.6 ng/ml.

NOEV up to 7 days. NOEV was saturated in the brain, liver and kidney within 3–7 days. NOEV in these tissues and body fluids (plasma and urine) disappeared within 4–7 days after chase with water without NOEV. The level of NOEV concentration remained essentially unchanged in a small number of mice during the experimental period up to 6 months (Fig. 2). The NOEV concentration in the brain was about 10% of that in the liver and kidney. Plasma concentration remained low, and NOEV was mainly secreted in the urine after continuous NOEV administration for 6 months (data not shown).

3.4. β-Gal activity

In parallel with the NOEV concentration, β-gal activity remained stable in Tg mouse tissues during the course of NOEV treatment (1 week–6 months) (data not shown). β-Gal activity in the Tg mouse brain was enhanced to 20–25% of the WT mouse brain after treatment with NOEV for 2–5 months (Fig. 3). The enzyme activity was elevated to the normal level in the kidney, and significantly higher than normal in the liver.

3.5. Clinical effect

The NOEV treatment was started at 1–2 months after birth (Fig. 4). Dose-dependent changes of assessment scores were observed in the three Tg mouse groups in this study; 0.1 mM NOEV (low dose; $N=11$), 0.3 mM NOEV (medium dose; $N=12$) and 1 mM NOEV (high dose; $N=6$). The roughly calculated daily NOEV dose was 6.5 mg/kg/day, 20 mg/kg/day, and 65 mg/kg/day, respectively. Among the three groups, the high-dose NOEV group showed a remarkable arrest of the increase in assessment scores as compared to the water group within a few months after starting treatment. The other two groups also showed highly significant effects with less remarkable arrest of progression.

Survival time was significantly prolonged in the 0.1 mM and 0.3 mM groups as compared to the water group (Table 3). However, the 1 mM group showed no significant prolongation in spite of a remarkable clinical effect as shown in Fig. 3. Further, higher doses of NOEV administration (3 mM and 10 mM) resulted in apparently shorter survival time, but statistical analysis was not performed because of small mouse numbers.

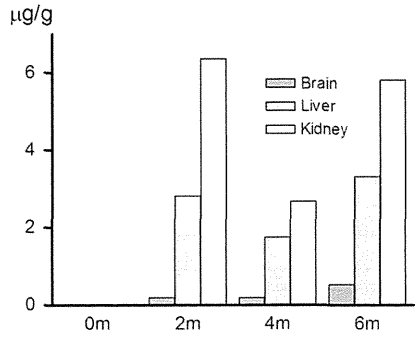

Fig. 2. Tissue concentrations during long-term NOEV treatment. R201C Tg mouse tissues (n = 2) were subjected to NOEV determination every two months as described in Section 2.4. Some variations were observed in individual samples. However, no remarkable chronological changes were noted in the brain, liver or kidney.

3.6. Blood chemistry and urinalysis

GOT and GPT were high in some WT, Tg, or KO mice with or without 1 mM NOEV treatment. They were not correlated with the genotype, clinical course, age, or NOEV treatment. BUN and creatinine,

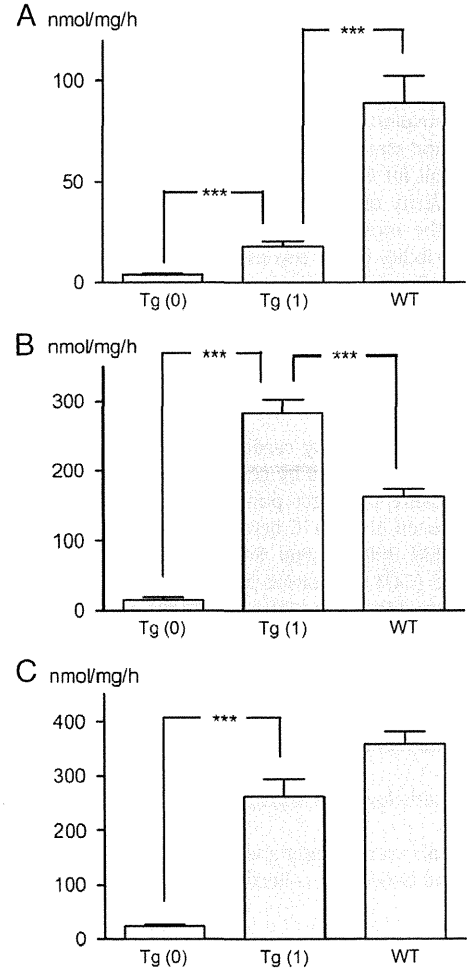

Fig. 3. β-Gal activity in the brain (A), liver (B), and kidney (C) of Tg and WT mice with or without NOEV treatment (1 mM solution orally ad libitum). Tg(0) = Tg mice without NOEV treatment (age 7–14 months, N = 8), Tg(1) = NOEV-treated Tg mice (age 7–14 months, NOEV treatment for 2–5 months, N = 8), WT = WT mice without NOEV treatment (age 7–14 months, N = 5). Each column indicates mean ± SEM. Enzyme activity is expressed as nmol of 4-methylumbelliferone/mg protein/h. Statistical analysis: $p=0.0002$ for Tg(0) vs Tg(1), and $p=0.0016$ for T(1) vs WT in the brain; $p=0.0009$ for Tg(0) vs Tg(1), and $p=0.0043$ for Tg(1) and WT in the liver; $p=0.0002$ for Tg(0) vs Tg(1), and $p=0.1274$ for Tg(1) vs WT in the kidney.

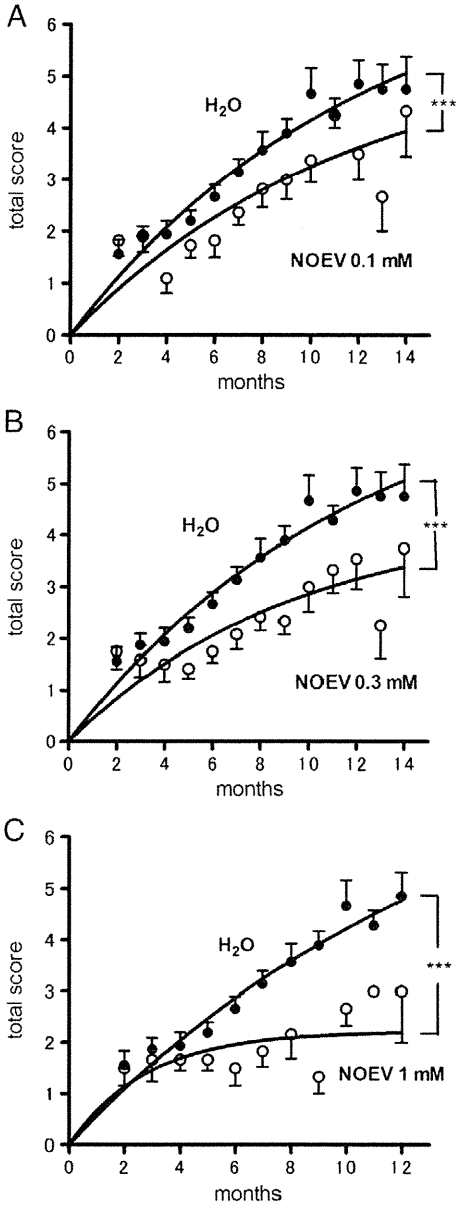

Fig. 4. Neurological assessment of NOEV-treated G_{M1}-gangliosidosis model mice (R201C Tg mice). After starting oral NOEV administration ad libitum at 1–2 months after birth, the three assessment tests were performed every month in individual mice, and total scores were recorded. The scores for each treatment group were compared with those for the non-treatment (water) group of the same age. Each value indicates mean ± SEM. Statistical analysis (two-way ANOVA) revealed $p<0.0001$ for water mice ($N=16$) vs 0.1 mM (low dose) NOEV mice ($N=11$) (A); $p<0.0001$ for water mice ($N=16$) vs 0.3 mM (medium dose) NOEV mice ($N=12$) (B); and $p<0.0001$ for water mice ($N=16$) vs 1 mM NOEV (high dose) mice ($N=6$) (C). NOEV dose was estimated on the basis of body weight and mean daily water intake: 6.5 mg/kg/day in 0.1 mM NOEV mice, 20 mg/kg/day in 0.3 mM NOEV mice, and 65 mg/kg/day in 1 mM NOEV mice.

urinary protein and occult blood, and other markers related to renal function were all normal (data not shown).

3.7. Pathology and immunohistochemistry

Neuronal cell degeneration was significantly improved in the mice treated with 1 mM NOEV for 2–7 months (Table 4). One case of 10 mM NOEV administration also showed a marked arrest of degeneration within 2 months of NOEV therapy. Immunohistochemical stain revealed a marked decrease in G_{M1} storage in NOEV-treated Tg mice, although the statistical analysis was not performed because of small numbers of cases (Table 4).

Table 3
NOEV effect on survival time.

NOEV	N	Survival (median)		Effect[a]
0 mM	26	5–16 m	(11 m)	–
0.1 mM	11	11–22 m	(14 m)	S(0.1) > S(0) (p = 0.0090)
0.3 mM	12	11–18 m	(14 m)	S(0.3) > S(0) (p = 0.0082)
1 mM	7	8–16 m	(10 m)	S(1) ≈ S(0) (p = 0.2102)
3 mM	3	8–10 m	(8 m)	S(3) ≤ S(0)[b]
10 mM	2	2–3 m	(2.5 m)	S(10) < S(0)[b]

R201C Tg mice on various concentrations of NOEV were compared.
S(0) = survival on water, S(0.1) = survival on 0.1 mM NOEV, S(0.3) = survival on 0.3 mM NOEV, S(1) = survival on 1 mM NOEV, S(3) = survival on 3 mM NOEV, S(10) = survival on 10 mM NOEV.
[a] Gehan–Breslow–Wilcoxon test.
[b] No statistical analysis because of small sample numbers.

General pathology showed no specific changes in NOEV-treated mouse tissues as compared to those from non-treated mice. Representative results are summarized for the liver, kidney, pancreas, and thymus (Table 4). Degeneration of hepatic cells, renal tubular cells, Langerhans cells, and thymus was observed in some mice in both treated and non-treated groups. We noticed a slight increase of tubular degeneration in the kidney of mice treated with 1 mM NOEV for 5–7 month, whereas a remarkable tubular degeneration was observed in a high-dose treatment mouse (10 mM NOEV for 2 months).

4. Discussion

G_{M1}-gangliosidosis is a relatively rare disease. The incidence was estimated to be 1:100,000–200,000 live births [26,27]. It is the 4th common sphingolipidosis in Turkey [28]. The chaperone effect is gene mutation-specific. After our report on the β-gal cDNA cloning [1], more than 160 mutations have been identified [2,27,29–31]. Mutations in G_{M1}-gangliosidosis patients are heterogeneous and complex. No ethnic prevalence has been known although some common mutations have been identified: p.R482H in Italian patients with infantile G_{M1}-gangliosidosis; p.R208C in American patients with infantile G_{M1}-gangliosidosis; p.R201C in Japanese patients with juvenile G_{M1}-gangliosidosis; and p.I51T in Japanese patients with adult G_{M1}-gangliosidosis [2]. Another mutation p.W273L is known to cause Morquio B disease [4].

Table 4
Semi-quantitative pathological scores after NOEV treatment (R201C Tg mouse).

	NOEV	0 mM	1 mM	10 mM	Score range
Neuropathology	Neuron[a]	4.80 (n = 10)	3.57 (n = 7)**	3 (n = 1)	1–5
	G_{M1}[b]	3.00 (n = 3)	1.25 (n = 4)	–	1–5
General pathology	Liver[c]	0.50 (n = 10)	0.71 (n = 7)	1 (n = 1)	0–3
	Kidney[c]	0.40 (n = 10)	0.57 (n = 7)	3 (n = 1)	0–3
	Pancreas[c]	0.20 (n = 10)	0.57 (n = 7)	1 (n = 1)	0–3
	Thymus[c]	0.30 (n = 10)	1.14 (n = 7)	2 (n = 1)	0–3

NOEV treatment (p.o., ad libitum) for 2–7 months (1 mM; age 4–11 months) or 2 months (10 mM; age 4 months). Each figure indicates the mean score in each group. **p = 0.0013 (0 mM vs 1 mM). No statistical difference or not tested in other groups.
[a] Neuronal degeneration: 0 = normal, 1 = vacuolation/degeneration <25%, 2 = vacuolation/degeneration <50%, 3 = vacuolation/degeneration <75%, 4 = vacuolation/degeneration <100%, 5 = extreme neuronal loss and gliosis/severe vacuolation and degeneration of remaining neurons.
[b] G_{M1} storage: 0 = no storage (normal), 2 = slight storage, 3 = moderate storage (TG mouse level at the end stage), 4 = high storage, 5 = extremely high storage (KO mouse level at the end stage).
[c] Liver: degeneration of hepatocytes, kidney: degeneration/dilatation of renal tubules, pancreas: degeneration of Langerhans cells, thymus: atrophy with loss of lymphocytes. Four semi-quantitative grades based on regular microscopic observations: 0 = normal, 1 = slightly abnormal, 2 = moderately abnormal, 3 = highly abnormal.

Various experimental therapeutic approaches have been reported toward G_{M1}-gangliosidosis. A thiol protease inhibitor prolonged the effect of exogenous β-gal in human G_{M1}-gangliosidosis fibroblasts [32]. The effect was enhanced when the enzyme was supplied as liposomes. Enzyme replacement of cultured cells from cats with G_{M1}-gangliosidosis was tried with the liposome-entrapped enzyme, and the storage of glycopeptides decreased [33]. Allogeneic bone marrow transplantation was performed in a Portuguese water dog affected with G_{M1}-gangliosidosis using a dog leukocyte antigen-identical sibling as donor [33]. β-Gal activity in leukocytes of the transplanted dog was similar to that in the donor. However, neither the subsequent clinical course nor the enzyme activity was modified. Beneficial effects of substrate reduction therapy were obtained in a mouse model of G_{M1}-gangliosidosis [34]. Galactose has been reported to be a potential chemical chaperone in some G_{M1}-gangliosidosis mutations as well as in Fabry disease [35].

At present no clinical therapeutic trial has been reported for G_{M1}-gangliosidosis. We have tried to develop a molecular therapeutic technology based on a new concept (chaperone therapy) toward a few lysosomal diseases as first examples [8,10,14,36]. An exogenous competitive inhibitor of a lysosomal enzyme binds to the mutant enzyme protein to form a stable complex at neutral pH of the rough endoplasmic reticulum–Golgi compartment. The enzyme-chaperone complex is safely transported to the lysosome, and dissociated under the acidic condition and in the presence of excessive storage of the substrate. The mutant enzyme remains stabilized, expressing catalytic function [5].

First we used cultured cells from Fabry patients with generalized vasculopathy [6,8,10], and then turned our attention to G_{M1}-gangliosidosis, a classic neurogenetic disease mainly occurring in infancy and childhood [14]. We started an extensive survey of chaperones for β-gal, but no commercially available compound was found to be sufficiently effective to β-gal. DGJ was effective to some extent, but we needed a much higher dose for G_{M1}-gangliosidosis than for Fabry disease [37]. Then we found a new galacto-type valienamine derivative produced by organic synthesis as a β-gal inhibitor [13]. It exhibited potent inhibitory and chaperone activities toward the human enzyme [14]. The octyl derivative NOEV showed the highest chaperone activity, and its hydrochloride salt was found to be easily soluble in water. We used the water solution of NOEV hydrochloride for subsequent experiments.

Molecular modeling of human β-gal protein was reported on the basis of *Penicillium* sp. enzyme structure with some theoretical insight on mutant proteins and enzyme–chaperone interactions [30,38,39]. Our preliminary computational calculation indicated that the binding free energy between NOEV and enzyme is higher at acidic pH in the lysosome than that at neutral pH in the endoplasmic reticulum-Golgi apparatus [5,23,38], thus suggesting that the enzyme protein is more easily dissociated from the enzyme-chaperone complex in the lysosome, stays stable, and exhibits catalytic activity. Recently three-dimensional crystal structure of the human enzyme was reported [40]. We expect that this information will further promote our understanding of chaperone biology in the near future.

After preliminary studies on culture cells, we chose 1 mM NOEV solution for chaperone therapy experiments on G_{M1}-gangliosidosis model mice [14]. Oral administration of NOEV demonstrated delivery to the central nervous system through the blood–brain barrier to enhance the β-gal activity and to reduce the substrate storage in this study as well as in previous preliminary studies [14,15] within a few days after starting oral administration. NOEV disappeared within a few days after cessation of oral administration. There was no tendency of intracellular accumulation. The data in this report suggests that NOEV is largely excreted in the urine through the kidney possibly without structural modification of the compound molecule, although its metabolites were not specifically searched for in this study.

In parallel with an increase of NOEV in neural and non-neural tissues, β-gal activity increased remarkably to normal or even higher level, particularly in the liver. The enzyme activity reached 20–25% of normal level in the brain. We have no data on the molecular mechanism of delivery of this galactose analog compound to the brain. The molecule is small in size, with both hydrophilic and hydrophobic structures, and any of the galactose transporters may well be involved in delivery through the blood–brain barrier.

For clinical assessment of the chaperone effect on experimental model mice on NOEV treatment, we developed simple motor and reflex testing methods that can be used manually without any special instruments. At first we took 11–16 different tests [23], then selected the three more specified tests avoiding overlaps of the test results in this study. Tail posture is a very sensitive sign of early brain damage (data not shown). Tail hanging demonstrated hind limb extension equivalent to a well-documented parachute reflex in normal human infants and children [21]. Further we examined missteps (formerly horizontal wire netting [15]) on a horizontally placed wire mesh. It was a sensitive method to detect abnormality in equilibrium and reflex grasping strength after the mid-stage of the disease. This is a test similar to that described by Papaioannou [22]. We calculated total scores of these three tests, which were reliable and reproducible to estimate progression of the reflex-motor aspect of the brain damage in G_{M1}-gangliosidosis mice. We did not try to evaluate the higher cortical function. In this assessment system, a relatively high dose of 1 mM NOEV treatment showed a remarkable effect for arrest of the disease progression within a few months after starting NOEV administration. Treatment of lower doses (0.1 mM and 0.3 mM) resulted in less impressive results, although all these three doses gave highly significant differences statistically as compared to non-treated mice. Neuropathology and immunohistochemistry supported these clinical findings, indicating less severe neuronal degeneration and decrease of G_{M1} storage. Early treatment was absolutely necessary to achieve such a dramatic result. Treatment at the late stage of the disease was clinically not effective. We did not start the treatment in the neonatal period immediately after birth for technical reasons to feed the water solution before weaning.

In spite of these neurological findings, effects on survival time were less remarkable particularly in the high-dose group (1 mM NOEV = 75 mg/kg/day) as compared to the medium-dose group (0.3 mM NOEV = 20 mg/kg/day) or low-dose group (0.1 mM NOEV = 6.5 mg/kg/day). In order to investigate the reason of this apparent discrepancy between the neurological effect and survival time, we analyzed carefully pathological and clinical laboratory data. Renal tubular changes were the only noticeable abnormality we could detect in general pathology in one case of very high dose NOEV treatment (10 mM NOEV = 650 mg/kg/day). This may have affected the life survival in large dose mouse groups.

In conclusion NOEV is definitely effective to prevent the progression of brain pathology at low doses, although we need to evaluate the possible subclinical adverse effect(s) on extraneural tissues in more detail, particularly on the renal tissue at high-dose treatment. Still, low-dose NOEV treatment will be sufficient to prevent disease progression of the central nervous system in G_{M1}-gangliosidosis if started early in life. Judging from the data in this study we suggest that the daily dose of 30–50 mg/kg or less will be appropriate in mice. Also intermittent administration, such as alternate day therapy, will be practically more feasible for reduction of the treatment dose, as the chaperone effect of NOEV lasts at least 2 days without supplementation. Prenatal chaperone therapy may be possible to supply the intrauterine fetus with NOEV through the placenta by its administration to the pregnant mother. There is no experimental data on this therapeutic possibility at present. We hope that chaperone therapy will be a new molecular therapy for prevention of progressive brain disease among a large number of human genetic diseases, as no effective therapy has been documented at present for any primary

neurogenetic disease. This is the first scientific approach to a rare but theoretically significant neurogenetic disease in children.

Conflict of interest

There is no conflict of interest in this work.

Acknowledgments

This study was supported by grants from the Ministry of Health, Labor and Welfare (H17-Kokoro-019, H20-Kokoro-022, H19-Nanji-Ippan-002, H22-Nanji-Ippan-002) and a grant from Japan Science and Technology Agency (AS232Z00009G).

References

[1] A. Oshima, A. Tsuji, Y. Nagao, H. Sakuraba, Y. Suzuki, Cloning, sequencing, and expression of cDNA for human β-galactosidase, Biochem. Biophys. Res. Commun. 157 (1988) 238–244.
[2] Y. Suzuki, E. Nanba, J. Matsuda, K. Higaki, A. Oshima, β-Galactosidase deficiency (β-galactosidosis): G_{M1}-gangliosidosis and Morquio B disease, in: D. Valle, A.L. Beaudet, B. Vogelstein, K.W. Kinzler, S.F. Antonarakis, A. Ballabio (Eds.), The Online Metabolic and Molecular Bases of Inherited Disease, McGraw-Hill, New York, 2008, pp. 1–101 http://www.ommbid.com.
[3] K. Yoshida, A. Oshima, M. Shimmoto, Y. Fukuhara, H. Sakuraba, N. Yanagisawa, Y. Suzuki, Human β-galactosidase gene mutations in G_{M1}-gangliosidosis: a common mutation among Japanese adult/chronic cases, Am. J. Hum. Genet. 49 (1991) 435–442.
[4] A. Oshima, K. Yoshida, M. Shimmoto, Y. Fukuhara, H. Sakuraba, Y. Suzuki, Human β-galactosidase gene mutations in morquio B disease, Am. J. Hum. Genet. 49 (1991) 1091–1093.
[5] Y. Suzuki, S. Ogawa, Y. Sakakibara, Chaperone therapy for neuronopathic lysosomal diseases: competitive inhibitors as chemical chaperones for enhancement of mutant enzyme activities, Perspect. Med. Chem. 3 (2009) 7–19.
[6] S. Ishii, R. Kase, H. Sakuraba, Y. Suzuki, Characterization of a mutant α-galactosidase gene product for the late-onset cardiac form of Fabry disease, Biochem. Biophys. Res. Commun. 197 (1993) 1585–1589.
[7] T. Okumiya, S. Ishii, R. Kase, S. Kamei, H. Sakuraba, Y. Suzuki, α-Galactosidase gene mutations in Fabry disease: heterogeneous expressions of mutant enzyme proteins, Hum. Genet. 95 (1995) 557–561.
[8] T. Okumiya, S. Ishii, T. Takenaka, R. Kase, S. Kamei, H. Sakuraba, Y. Suzuki, Galactose stabilizes various missense mutants of α-galactosidase in Fabry disease, Biochem. Biophys. Res. Commun. 214 (1995) 1219–1224.
[9] A. Frustaci, C. Chimenti, R. Ricci, L. Natale, M.A. Russo, M. Pieroni, C.M. Eng, R.J. Desnick, Improvement in cardiac function in the cardiac variant of Fabry's disease with galactose-infusion therapy, N. Engl. J. Med. 345 (2001) 25–32.
[10] J.Q. Fan, S. Ishii, N. Asano, Y. Suzuki, Accelerated transport and maturation of lysosomal α-galactosidase A in Fabry lymphoblasts by an enzyme inhibitor, Nat. Med. 5 (1999) 112–115.
[11] Y. Suzuki, β-Galactosidase deficiency: an approach to chaperone therapy, J. Inherit. Metab. Dis. 29 (2006) 471–476.
[12] S. Ogawa, Y. Kobayashi, K. Kabayama, M. Jimbo, J. Inokuchi, Chemical modification of β-glucocerebrosidase inhibitor *N*-octyl-β-valienamine: synthesis and biological evaluation of *N*-alkanoyl and *N*-alkyl derivatives, Bioorg. Med. Chem. 6 (1998) 1955–1962.
[13] S. Ogawa, Y.K. Matsunaga, Y. Suzuki, Chemical modification of the β-glucocerebrosidase inhibitor *N*-octyl-β-valienamine: synthesis and biological evaluation of 4-epimeric and 4-O-(β-D-galactopyranosyl) derivatives, Bioorg. Med. Chem. 10 (2002) 1967–1972.
[14] J. Matsuda, O. Suzuki, A. Oshima, Y. Yamamoto, A. Noguchi, K. Takimoto, M. Itoh, Y. Matsuzaki, Y. Yasuda, S. Ogawa, Y. Sakata, E. Nanba, K. Higaki, Y. Ogawa, L. Tominaga, K. Ohno, H. Iwasaki, H. Watanabe, R.O. Brady, Y. Suzuki, Chemical chaperone therapy for brain pathology in G_{M1}-gangliosidosis, Proc. Natl. Acad. Sci. U. S. A. 100 (2003) 15912–15917.
[15] Y. Suzuki, S. Ichinomiya, M. Kurosawa, M. Ohkubo, H. Watanabe, H. Iwasaki, J. Matsuda, Y. Noguchi, K. Takimoto, M. Itoh, M. Tabe, M. Iida, T. Kubo, S. Ogawa, E. Nanba, K. Higaki, K. Ohno, R.O. Brady, Chemical chaperone therapy: clinical effect in murine G_{M1}-gangliosidosis, Ann. Neurol. 62 (2007) 671–675.
[16] S. Ogawa, H. Tsunoda, J. Inokuchi, Synthesis of glucosylceramide analogues: imino-linked 5a-carbaglycosylceramides, potent and specific glucocerebrosidase inhibitors, J. Chem. Soc. Chem. Commun. (1994) 1317–1318.
[17] H. Tsunoda, J. Inokuchi, K. Yamagishi, S. Ogawa, Synthesis of glycosylceramide analogs composed of imino-linked unsaturated 5a-carbaglycosyl residues: potent and specific gluco- and galactocerebrosidase inhibitors, Liebigs Annal. Chem. (1995) 279–284.
[18] S. Ogawa, M. Ashiura, C. Uchida, S. Watanabe, C. Yamazaki, K. Yamagishi, J.-I. Inokuchi, Synthesis of potent β-D-glucocerebrosidase inhibitors: *N*-alkyl-β-valienamines, Bioorg. Med. Chem. Lett. 6 (1996) 929–932.
[19] J. Matsuda, O. Suzuki, A. Oshima, A. Ogura, Y. Noguchi, Y. Yamamoto, T. Asano, K. Takimoto, K. Sukegawa, Y. Suzuki, M. Naiki, β-Galactosidase-deficient mouse as an animal model for G_{M1}-gangliosidosis, Glycoconj. J. 14 (1997) 729–736.
[20] H. Iwasaki, H. Watanabe, M. Iida, S. Ogawa, M. Tabe, K. Higaki, E. Nanba, Y. Suzuki, Fibroblast screening for chaperone therapy in β-galactosidosis, Brain Dev. 28 (2006) 482–486.
[21] J. Matsuda, O. Suzuki, A. Oshima, A. Ogura, M. Naiki, Y. Suzuki, Neurological manifestations of knockout mice with β-galactosidase deficiency, Brain Dev. 19 (1997) 19–20.
[22] V.E. Papaioannou, R.R. Behringer, Mouse phenotypes, A Handbook of Mutation Analysis, Cold Spring Harbor Laboratory Press, New York, 2005.
[23] S. Ichinomiya, H. Watanabe, K. Maruyama, H. Toda, H. Iwasaki, M. Kurosawa, J. Matsuda, Y. Suzuki, Motor and reflex testing in G_{M1}-gangliosidosis model mice, Brain Dev. 29 (2007) 210–216.
[24] M. Taniguchi, Y. Shinoda, H. Ninomiya, M.T. Vanier, K. Ohno, Sites and temporal changes of gangliosides G_{M1}/G_{M2} storage in the Niemann–Pick disease type C mouse brain, Brain Dev. 23 (2001) 414–421.
[25] S. Ogawa, Y. Sakata, N. Ito, M. Watanabe, K. Kabayama, M. Itoh, T. Korenaga, Convenient synthesis and evaluation of glycosidase inhibitory activity of α and β-galactose-type valienamines, and some *N*-alkyl derivatives, Bioorg. Med. Chem. 12 (2004) 995–1002.
[26] P.J. Meikle, J.J. Hopwood, A.E. Clague, W.F. Carey, Prevalence of lysosomal storage disorders, JAMA 281 (1999) 249–254.
[27] A. Caciotti, S.C. Garman, Y. Rivera-Colon, E. Procopio, S. Catarzi, L. Ferri, C. Guido, P. Martelli, R. Parini, D. Antuzzi, R. Battini, M. Sibilio, A. Simonati, E. Fontana, A. Salviati, G. Akinci, C. Cereda, C. Dionisi-Vici, F. Deodato, A. d'Amico, A. d'Azzo, E. Bertini, M. Filocamo, M. Scarpa, M. di Rocco, C.J. Tifft, F. Ciani, S. Gasperini, E. Pasquini, R. Guerrini, M.A. Donati, A. Morrone, G_{M1}-gangliosidosis and Morquio B disease: an update on genetic alterations and clinical findings, Biochim. Biophys. Acta 1812 (2011) 782–790.
[28] H.A. Ozkara, M. Topcu, Sphingolipidoses in Turkey, Brain Dev. 26 (2004) 363–366.
[29] D. Hofer, K. Paul, K. Fantur, M. Beck, A. Roubergue, A. Vellodi, B.J. Poorthuis, H. Michelakakis, B. Plecko, E. Paschke, Phenotype determining alleles in G_{M1}-gangliosidosis patients bearing novel *GLB1* mutations, Clin. Genet. 78 (2010) 236–246.
[30] K. Higaki, L. Li, U. Bahrudin, S. Okuzawa, A. Takamuram, K. Yamamoto, K. Adachi, R.C. Paraguison, T. Takai, H. Ikehata, L. Tominaga, I. Hisatome, M. Iida, S. Ogawa, J. Matsuda, H. Ninomiya, Y. Sakakibara, K. Ohno, Y. Suzuki, E. Nanba, Chemical chaperone therapy: chaperone effect on mutant enzyme and cellular pathophysiology in β-galactosidase deficiency, Hum. Mutat. 32 (2011) 843–852.
[31] N. Brunetti-Pierri, F. Scaglia, G_{M1}-gangliosidosis: review of clinical, molecular, and therapeutic aspects, Mol. Genet. Metab. 94 (2008) 391–396.
[32] Y.M. Ko, T. Yamanaka, M. Umeda, Y. Suzuki, Effects of thiol protease inhibitors on intracellular degradation of exogenous β-galactosidase in cultured human skin fibroblasts, Exp. Cell. Res. 148 (1983) 525–529.
[33] J.S. O'Brien, R. Storb, R.F. Raff, J. Harding, F. Appelbaum, S. Morimoto, Y. Kishimoto, T. Graham, A. Ahern-Rindell, S.L. O'Brien, Bone marrow transplantation in canine G_{M1}-gangliosidosis, Clin. Genet. 38 (1990) 274–280.
[34] E. Elliot-Smith, A.O. Speak, E. Lloyd-Evans, D.A. Smith, A.C. van der Spoel, M. Jeyakumar, T.D. Butters, R.A. Dwek, A. d'Azzo, F.M. Platt, Beneficial effects of substrate reduction therapy in a mouse model of G_{M1}-gangliosidosis, Mol. Genet. Metab. 94 (2008) 204–211.
[35] A. Caciotti, M.A. Donati, A. d'Azzo, R. Salvioli, R. Guerrini, E. Zammarchi, A. Morrone, The potential action of galactose as a "chemical chaperone": increase of β-galactosidase activity in fibroblasts from an adult G_{M1}-gangliosidosis patient, Eur. J. Paediatr. Neurol. 13 (2009) 160–164.
[36] H. Lin, Y. Sugimoto, Y. Ohsaki, H. Ninomiya, A. Oka, M. Taniguchi, H. Ida, Y. Eto, S. Ogawa, Y. Matsuzaki, M. Sawa, T. Inoue, K. Higaki, E. Nanba, K. Ohno, Y. Suzuki, *N*-octyl-β-valienamine up-regulates activity of F213I mutant β-glucosidase in cultured cells: a potential chemical chaperone therapy for Gaucher disease, Biochim. Biophys. Acta 1689 (2004) 219–228.
[37] L. Tominaga, Y. Ogawa, M. Taniguchi, K. Ohno, J. Matsuda, A. Oshima, Y. Suzuki, E. Nanba, Galactonojirimycin derivatives restore mutant human β-galactosidase activities expressed in fibroblasts from enzyme-deficient knockout mouse, Brain Dev. 23 (2001) 284–287.
[38] H. Jo, K. Yugi, S. Ogawa, Y. Suzuki, Y. Sakakibara, Molecular basis of chemical chaperone effects of *N*-octyl-β-valienamine on human β-glucosidase in low/neutral pH conditions, J. Proteomics Bioinformat 3 (2010) 104–112.
[39] M. Morita, S. Saito, K. Ikeda, K. Ohno, K. Sugawara, T. Suzuki, T. Togawa, H. Sakuraba, Structural bases of G_{M1}-gangliosidosis and Morquio B disease, J. Hum. Genet. 54 (2009) 510–515.
[40] U. Ohto, K. Usui, T. Ochi, K. Yuki, Y. Satow, T. Shimizu, Crystal structure of human β-galactosidase: The structural basis of G_{M1}-gangliosidosis and Morquio B diseases, J. Biol. Chem. 287 (2012) 1801–1812.

DECREASED SURFACE SIALIC ACID CONTENT IS A SENSITIVE INDICATOR OF MUSCLE DAMAGE

YUKO IWATA, PhD,[1] OSAMU SUZUKI, PhD,[2] and SHIGEO WAKABAYASHI, PhD[1]

[1] Department of Molecular Physiology, National Cerebral and Cardiovascular Center Research Institute, Fujishiro-dai 5-7, Suita, Osaka 565-8565, Japan

[2] Laboratory of Animal Models for Human Diseases, National Institute of Biomedical Innovation, Ibaraki, Osaka, Japan

Accepted 12 August 2012

ABSTRACT: *Introduction*: The glycosylation state of the muscle sarcolemma is crucial for membrane strength and is thereby linked to pathologic conditions. No markers currently exist with sufficient sensitivity to detect muscle damage in biopsy samples. We aimed to determine whether surface sialic acid content is a useful criterion for estimating muscle injury. *Methods*: Sialic acid content was measured by comparing the fluorescence intensity of muscle sections stained with 2 types of lectins. One binds specifically to nonsialylated sugars, and the other binds to both sialylated and nonsialylated sugars. *Results*: Sialic acid levels were markedly reduced (60–80%) in muscles from dystrophin-defective mice, δ-sarcoglycan–deficient hamsters, merosin-deficient mice, and patients with muscular dystrophy, when compared with their healthy counterparts. *Conclusions*: Testing for a marked decrease in sialic acid levels, which is caused by the release of trace amounts of sialidase from damaged muscles, is a sensitive detection method for muscle injury and could be commonly utilized for various subtypes of muscular dystrophy.

Muscle Nerve **47:** 372–378, 2013

Muscular dystrophy is a severe degenerative disorder of skeletal muscle, characterized by progressive muscle weakness.[1] One subgroup of this disease is caused by a defect in the genes that encode for the components of the dystrophin–glycoprotein complex (DGC). This multi-subunit complex spans the sarcolemma to structurally link extracellular matrix proteins, such as laminin, to the actin cytoskeleton, thereby providing mechanical strength to muscle cell membranes.[2,3] Therefore, defects of the DGC result in marked disruption of membrane integrity and/or stability. Sarcolemmal damage accelerates the release of cytoplasmic enzymes or the entry of extracellular substances across the cell membranes. To date, increased serum creatine kinase (CK)[4] levels have been used as an indicator of the extent of muscle damage in patients with Duchenne muscular dystrophy or in corresponding animal models such as dystrophin-deficient mice (*mdx*). However, measurement of serum CK levels is not always a reliable indicator of muscle damage, because they rise and fall rapidly and are easily affected by stresses to the body from surgical procedures, vigorous exercise, or deep intramuscular injections.[5–7] In addition, other cytosolic enzymes released in serum, such as myoglobin, aldolase, or lactate dehydrogenase, have similar limitations with regard to the detection of muscle damage. Furthermore, merosin-deficient mice (*dy/dy*), another dystrophic model representative of human merosin-deficient congenital muscular dystrophy, demonstrated no detectable increase in serum CK levels despite their severe clinical phenotype.[8] Enhanced uptake of externally added Evans blue dye (EBD)[8] as a marker of membrane integrity cannot be used in humans owing to its toxicity; even in animals only postmortem muscle imaging is possible using EBD.

Establishing a diagnosis of muscle damage using biopsy samples and routine analysis is time consuming, even in distinguishing between myopathy and neuropathy. Therefore, newer and simpler methods would be useful for easy detection of muscle damage in various types of muscle degenerative disorders, and the validation of a new diagnostic marker would be invaluable.

Glycosylation has been demonstrated to be intimately linked to muscular dystrophy. Indeed, glycosylation of α-dystroglycan (α-dystroglycan DG), an essential component of the DGC, is critical for its interaction with the extracellular matrix to preserve the mechanical strength of the sarcolemma. Moreover, α-DG interacts with extracellular matrix proteins such as laminin through *O*-mannosyl–linked sialylated tetrasaccharides.[9–11] Abnormal glycosylation of α-DG has been detected in multiple forms of muscular dystrophy in mice and humans.[12,13] Therefore, we hypothesized that a test for changes in glycosylation of the sarcolemma could be used for diagnostic purposes for various types of muscular dystrophy.

Sialic acid (a generic term for neuraminic acid derivatives) is an important carbohydrate expressed on the terminal ends of glycan structures in many cell surface glycoproteins and glycolipids, where they mediate various cellular functions (e.g., cell–cell or cell–matrix interactions)[14] and are essential for mammalian survival, development, and growth.[15,16] Sialic acids are ultimately

Abbreviations: ACL, *Amaranthus caudatus* lectin; α-DG, α-dystroglycan; CK, creatine phosphokinase; DAPI, 4′,6-diamidino-2-phenylindole dihydrochloride; DGC, dystrophin–glycoprotein complex; *dy/dy*, merosin-deficient mice; EBD, Evans blue dye; FITC, fluorescein isothiocyanate; Galβ1,3GalNAc, galactose-(β1,3)-*N*-acetylgalactosamine; J2N-k, δ-sarcoglycan–deficient hamsters; J2N-n, control hamsters; *mdx*, dystrophin-deficient mice; PNA, peanut agglutinin; RT, room temperature; WT, wild-type

Key words: lectin staining, muscle injury, muscular dystrophy, sialic acid, sialidase

Correspondence to: Y. Iwata; e-mail: yukoiwat@ri.ncvc.go.jp

Published online 16 August 2012 in Wiley Online Library (wileyonlinelibrary.com). DOI 10.1002/mus.23632

transferred to oligosaccharide chains by the catalytic function of a large family of sialyltransferase enzymes. Conversely, the removal of sialic acid moieties is catalyzed by sialidase. The cytosolic fraction of skeletal muscles exhibits a higher level of sialidase activity than do other tissues.[17] Therefore, if sialidase is released from damaged muscle, it would greatly affect biological processes by changing the conformation of glycoproteins and uncovering or masking the binding sites of functional glycomolecules. Conversely, in distal myopathy with rimmed vacuoles (hereditary inclusion body myopathy), mutation of genes involved in the biosynthesis of sialic acids has been reported.[18–20] These findings raise the possibility that reduction in sialic acid levels has important pathological significance and may also be exploited as a sensitive detection method to monitor release of sialidase in various types of muscle degenerative disorders.

In this study, we addressed whether surface sialic acid content could be altered in muscular dystrophy.

METHODS

Materials. Biotinylated peanut agglutinin (PNA) lectin, *Amaranthus caudatus* lectin (ACL), and fluorescein isothiocyanate (FITC-avidin D; Vector Laboratories, Burlingame, California) were used according to manufacturer's instructions. The sialidase used was isolated from *Clostridium perfringens* (Sigma Chemical Co., St. Louis, Missouri). Alexa Fluor 647 goat anti-mouse IgG (H+L; Invitrogen, Carlsbad, California) and FITC-PNA (Vector Laboratories) were also used in several experiments.

Animals. Delta (δ)-sarcoglycan–deficient hamsters (J2N-k), a model of human δ-sarcoglycanopathy, and age-matched control hamsters (J2N-n) were purchased from Japan SLC, Inc. (Shizuoka, Japan). Four-week-old *dy/dy* and *mdx* mice and age-matched controls (wild-type [WT]) were purchased from the Jackson Laboratories (Bar Harbor, Maine). All animal experiments were performed in accordance with the animal experimentation guidelines of the National Cerebral and Cardiovascular Center (NCVC), Japan.

Human Tissues. Tissue samples were obtained from skeletal muscle biopsy specimens from the NCVC from patients with muscular dystrophy and by autopsies of patients without muscle failure as controls.[21] Written informed consent was obtained from all subjects.

Staining of Skeletal Muscle Sections with Lectins. The sugar chain properties in frozen sections (approximately 5–6 μm) of skeletal muscles were analyzed by the binding of biotinylated PNA or ACL, as described previously.[22] Frozen sections were fixed in 100% ethanol for 10 min at room temperature (RT). After washing with phosphate-buffered saline, the sections were incubated with each biotinylated lectin (10 μg/ml) for 15 min at RT. When sialidase treatment was performed, the sections were treated with 0–5000 mU of sialidase in 50 mM sodium acetate (pH 5) for 2 hours at 37°C before incubation with lectins. These lectins were visualized by incubating the sections with 20 μg/ml of FITC-avidin D for 5 min at RT, followed by observation under a fluorescence microscope (IX81; Olympus, Tokyo, Japan) equipped with confocal capability (Fluoview FV1000; Olympus). For greater time savings, the fixed sections were stained directly with FITC-PNA (10 μg/ml) for 15 min at RT. The nucleus was stained with 4′,6-diamidino-2-phenylindole dihydrochloride (DAPI; Dojindo Laboratories, Kamimashiki-gun, Japan).

Quantification of Fluorescent Intensity Visualized with Lectin Staining. Images of serial sections stained with lectins were analyzed by investigators blinded to the genotypes, using NIH Image software. The entire region covering each fiber and the region covering only the intracellular space in cross-sections were selected visually, and their fluorescence intensities were measured. Fluorescence intensity corresponding to the sarcolemmal region was calculated by subtracting the intensity of the intracellular region from that of the total area. All data were expressed as mean ± standard deviation (SD) unless otherwise indicated. Differences between the groups were determined using the Student *t*-test. $P < 0.05$ was considered statistically significant.

RESULTS

To specifically detect the sialylated sugar group, 2 types of lectins, PNA and ACL, were used. The PNA lectin specifically binds to nonsialylated galactose-(β1,3)-*N*-acetylgalactosamine (Galβ1,3GalNAc) moieties on oligosaccharide groups on glycoproteins or glycolipids, but not to sialylated sugar moieties (Fig. 1A). By contrast, ACL interacts with sialylated and nonsialylated forms of Galβ1,3GalNAc structures (Fig. 1A). Therefore, the amount of sialylated sugars can be measured easily by comparative staining between PNA and ACL in the plasma membrane (Fig. 1A). This strategy was applied to skeletal muscles from J2N-k and J2N-n hamsters. Skeletal muscles from both types of hamster were well stained with ACL (Fig. 1B and C), indicating that both types of sarcolemma express similar apparent levels of Galβ1,3GalNAc. By contrast, the

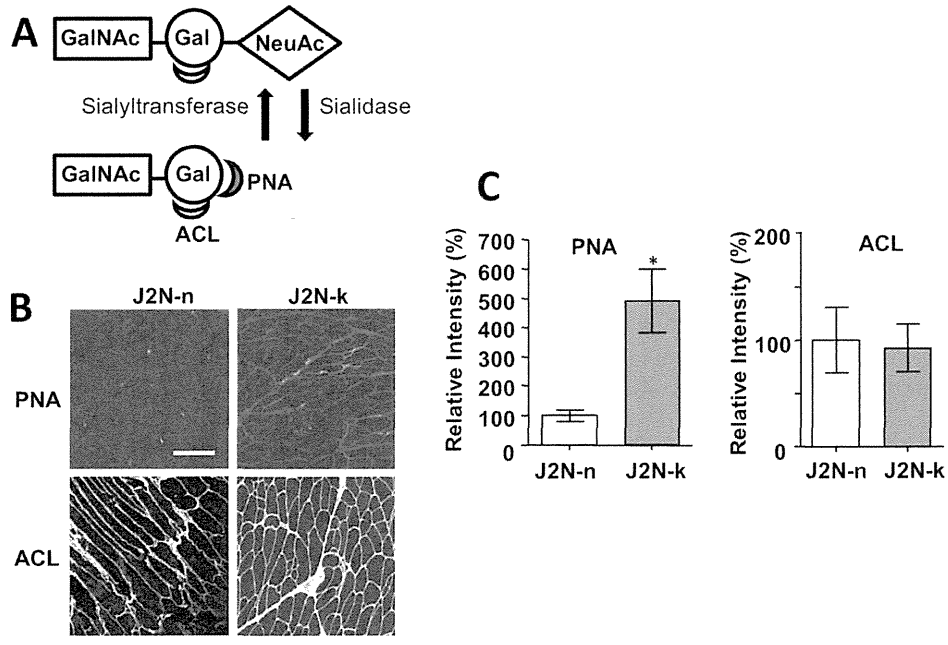

FIGURE 1. Increased PNA staining of J2N-k hamster muscles. (**A**) Schematic drawing representing the sialic acid–dependent or sialic acid–independent interaction of 2 types of lectins. Whereas ACL recognizes sialylated and nonsialylated sugars, PNA recognizes only nonsialylated sugars. NeuAc, neuraminic acid; Gal, D-galactose; GalNAc, *N*-acetyl-D-galactosamine. (**B**) Typical staining images with PNA or ACL. Frozen sections of quadriceps femoris muscle from dystrophic (J2N-k) and control hamsters (J2N-n) were stained with biotinylated PNA or ACL followed by FITC-avidin D. Scale bars: 50 μm. (**C**) Immunofluorescence images of myofiber cross-sections stained with lectins were analyzed by imaging software. Fluorescence intensity of each lectin staining was measured from 3 or 4 cross-sectional views of myofibers from 3 or 4 animals per group. Data were normalized with fluorescence in the J2N-n hamsters for each lectin. The data are presented as mean ± SD (n = 30–50 fibers/group). $^*P < 0.05$.

sarcolemmas from the J2N-k hamsters were more extensively stained with PNA compared with those from the J2N-n hamsters (Fig. 1B); the intensity of staining with PNA was approximately fivefold greater in the former than in the latter (Fig. 1C), indicating that the sarcolemmas from the J2N-k hamsters contained higher levels of nonsialylated sugars.

Stronger staining with PNA was also observed in muscle sections of *mdx* mice (Fig. 2A), with a PNA staining intensity that was approximately sixfold greater than that in the WT mice (Fig. 2B). Furthermore, when this staining method was applied to *dy/dy* mice, considerable staining with PNA was observed in the muscle sections (Fig. 2C); the staining intensity with PNA was approximately fourfold greater in *dy/dy* than in WT mice (Fig. 2D).

An important question is whether increased PNA staining occurs in necrotic fibers alone or throughout dystrophic muscles, which include normal and regenerating fibers. Intracellular IgG in the necrotic fibers was stained with anti-IgG antibody, as described previously,[8] whereas regenerating fibers with central nuclei were stained with DAPI. Intense PNA staining occurred everywhere in the *mdx* muscles (Fig. 3), including IgG-positive necrotic fibers, regenerating fibers with central nuclei, and normal fibers without central nuclei (see merged image in Fig. 3).

We applied the aforementioned staining procedure to the muscle biopsy samples from patients with muscular dystrophy (Fig. 4A and B). Whereas faint staining with PNA was observed in normal control muscles, muscle samples from patients with muscular dystrophy (Becker and/or limb-girdle muscular dystrophy) were strongly stained with PNA (Fig. 4A); the staining intensity with PNA was more than fourfold greater in muscles from patients with muscular dystrophy than in normal muscles (Fig. 4B). These data suggest that, similar to dystrophic animal models, muscle samples from patients with muscular dystrophy possess markedly reduced levels of sialic acids.

Muscular dystrophy results in sarcolemmal damage, which accelerates the release of cytosolic enzymes into the extracellular space. Therefore, it is probable that a sufficient amount of sialidase is released from injured muscles to remove sialic acids from the sarcolemma. To measure the catalytic action of sialidase, frozen sections of skeletal muscles from healthy mice were treated with externally added sialidase and subsequently stained with PNA. Sialidase treatment resulted in extensive staining of the muscle surface with PNA (Fig. 5A)

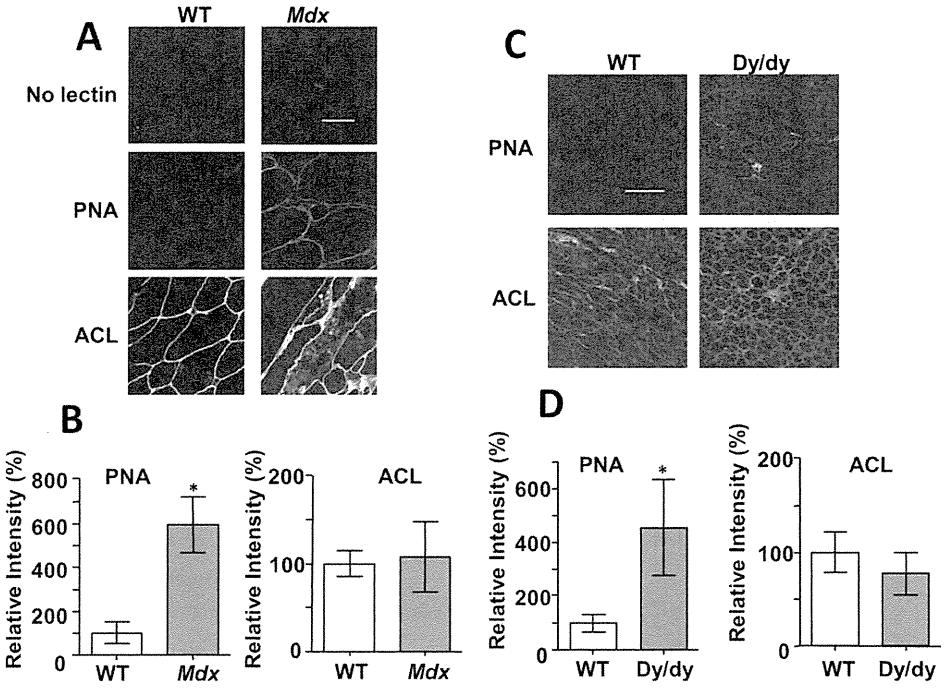

FIGURE 2. Increased PNA staining in the muscles of *mdx* and *dy/dy* mice. (**A**) Frozen sections of quadriceps femoris muscle from *mdx* (*Mdx*) and control mice (WT) were stained with biotinylated PNA or ACL followed by FITC-avidin D. Scale bars: 50 μm. (**B**) Immunofluorescence images of myofiber cross-sections stained with lectins were analyzed by imaging software, and fluorescence intensity was normalized to that of healthy mice. The data are presented as mean ± SD (n = 20–50 fibers/group); $^*P < 0.05$. (**C**) Frozen sections of quadriceps femoris muscle from *dy/dy* (*Dy/dy*) and control mice (WT) stained with biotinylated PNA or ACL, followed by FITC-avidin D. Scale bars: 50 μm. (**D**) Immunofluorescence images of myofiber cross-sections stained with lectins were analyzed by imaging software. Fluorescence intensity of each lectin staining was measured from 3 or 4 cross-sectional views of myofibers from 3 or 4 animals per group and normalized to that of healthy mice. The data are presented as mean ± SD (n = 40–50 fibers/group). $^*P < 0.05$.

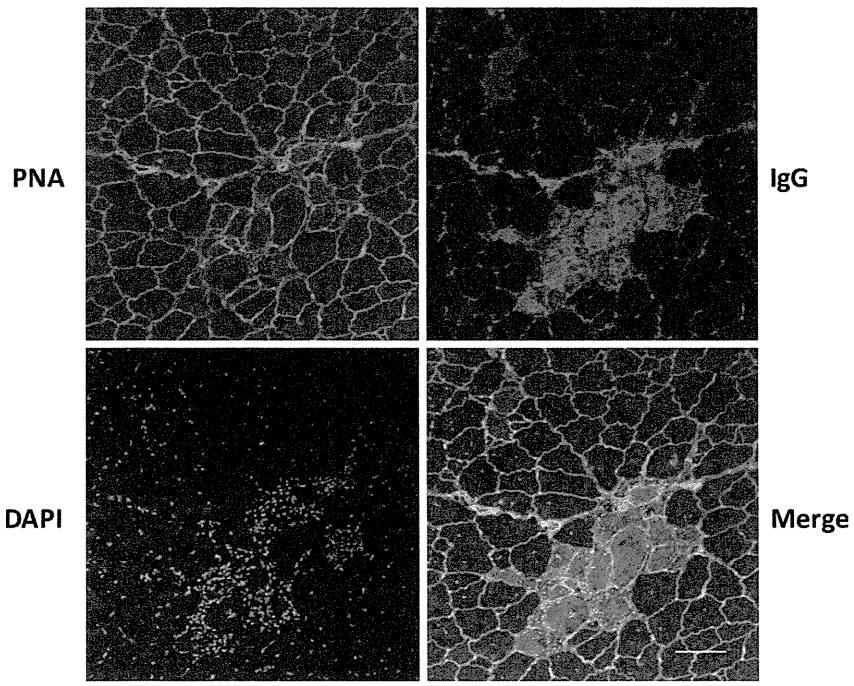

FIGURE 3. PNA staining is observed in all states of muscles, including necrotic fibers. Frozen sections of quadriceps femoris muscle from *mdx* mice were stained with FITC-PNA for sialic acids, DAPI for nuclei, and anti-mouse IgG for necrotic fibers. Scale bars: 50 μm. [Color figure can be viewed in the online issue, which is available at wileyonlinelibrary.com.]